Chapter 17

Finite Element Method for Structural Integrity Problems

Chapter details

Chapter DOI:

https://doi.org/10.4322/978-65-86503-83-8.c17

Chapter suggested citation / reference style:

Sales, Thiago P., et al. (2022). “Finite Element Method for Structural Integrity Problems”. *In* Jorge, Ariosto B., et al. (Eds.) *Fundamental Concepts and Models for the Direct Problem*, Vol. II, UnB, Brasilia, DF, Brazil, pp. 618–665. Book series in Discrete Models, Inverse Methods, & Uncertainty Modeling in Structural Integrity.

P.S.: DOI may be included at the end of citation, for completeness.

Book details

Book: Fundamental Concepts and Models for the Direct Problem

Edited by: Jorge, Ariosto B., Anflor, Carla T. M., Gomes, Guilherme F., & Carneiro, Sergio H. S.

Volume II of Book Series in:

Discrete Models, Inverse Methods, & Uncertainty Modeling in Structural Integrity

Published by: UnB City: Brasilia, DF, Brazil Year: 2022

DOI: https://doi.org/10.4322/978-65-86503-83-8

Finite Element Method for Structural Problems

Thiago de P. Sales[1*], Polliana C. O. Martins[2], Domingos A. Rade[3]

[1]Aeronautics Institute of Technology, Brazil, tpsales@ita.br
[2]University of Brasilia, Brazil, polliana.martins@unb.br
[3]Aeronautics Institute of Technology, Brazil, rade@ita.br

[*]Corresponding author

Abstract

The finite element method (FEM) has been applied to solve engineering problems in several areas during the last decades, fulfilling an important role, mainly in situations that present complex, or even non-existent, analytical solutions. As every numerical technique, this approach has limitations which are directly linked with digital computing capacity, since this method is widely and predominantly implemented using such tools. Thus, this chapter presents a contextualized and updated introduction to the FEM, including its fundamentals, such as important considerations about spatial discretization of the physical domain and formulation at element and global levels. Using the variational approach, the formulation of two different finite elements is presented in considerable depth, namely for a quadrilateral, two-dimensional elasticity FE, with four nodes; and for a Kirchhoff-Love plate, equivalent single layer composite/laminate FE, rectangular, with four nodes. In a second moment, two examples are discussed, the first of which is concerned with an H-shaped sheet, with one of its edges clamped, and being subject to a uniform pressure load. The second example studies a rectangular, four layer composite, clamped on one of its edges. By means of both of these, one highlights the importance of proper mesh generation and/or adequate selection of a FE for a given problem; as well as the various types of structural dynamics' analyzes one might be interested in performing. Additionally, most relevant information and discussion is provided concerning parameterization of FE models, particularly in association to model updating and damage identification. Particularly, a section is dedicated to model updating based on the sensitivity of eigenvalues and eigenvectors. Final remarks are also included, to point out most pertinent directions, in the view of the authors, for interested readers to follow. As a bonus, MATLAB® codes implemented by the authors, related to the two considered examples, are made available for download within the chapter material.

Keywords: Finite Element Method; quadrilateral two-dimensional finite element; rectangular Kirchhoff-Love plate; parameterization; model updating.

1 Introduction

From the Mathematics standpoint, the Finite Element Method (FEM) is a numerical technique intended to provided approximate solutions to differential equations. From the engineering perspective, the FEM has been conceived to obtain approximate solutions of a range of problems whose underlying physics are governed by differential equations. Despite the fact that the method has been originally developed for the analysis of structural systems, it has been widely used for the modeling of a variety of engineering problems, in the fields of Solid Mechanics, Fluid Mechanics, Heat Transfer, Electromagnetism, among others. Due to its accuracy, computational efficiency and modeling flexibility, besides its ease of implementation in digital computers, the FEM has achieved great diffusion, both in industry and academia, being considered as a high valued tool for the development of engineering projects and scientific investigations. One can surely say that the FEM is currently one of the most widely used numerical techniques in science and engineering. As a result, the method has been taught in most universities around the world, with the support of a variety of textbooks [Zimmerman, 2006, Lewis et al., 1996, Reddy, 2019, Jin, 2015, Bathe, 2014].

The main motivation for the use of the FEM lies in the fact that for highly complex Engineering problems, analytical solutions to the underlying differential equations are difficult – or even impossible – to obtain. In fact, mathematical models of those problems, represented by a single or a set of ordinary or partial differential equations, can be obtained from the application of well established physical principles governing the underlying phenomena. Very often, simplifications are adopted by neglecting effects considered to be less influential. However, the resolution of the governing equations by using classical mathematical techniques can be unfeasible due to existence of a number of complicating factors, such as complex geometry, combination of multiple materials, nonlinear behavior, variable material parameters (with time or environmental influences), etc. These complicating factors are very often present in actual industrial problems.

For illustration, let us consider the heat transfer problem on a thin plate, of arbitrary boundary shape and material composition, as illustrated in Fig. 1. As in many practical cases, simplification is made by assuming that, given that the plate is thin, temperature is constant across the thickness, which implies the absence of heat flux in that direction. Hence, the original three-dimensional problem is simplified to a two-dimensional counterpart.

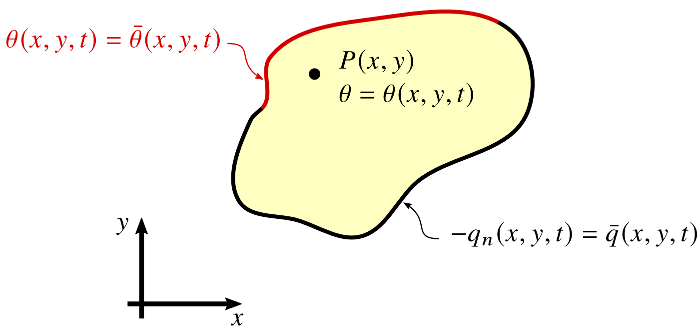

Figure 1: Illustration of a two-dimensional heat transfer problem on a plate of arbitrary shape.

Upon application of the law of energy conservation and Fourier's law of heat conduction to a differential element of the plate, the following partial differential equation, whose solution provides the transient temperature distribution over the plate, described by the so-called field variable, $\theta = \theta(x, y, t)$, is obtained:

$$\frac{\partial}{\partial x}\left(k_x(x, y, \theta)\frac{\partial \theta}{\partial x}\right) + \frac{\partial}{\partial y}\left(k_y(x, y, \theta)\frac{\partial \theta}{\partial y}\right) + Q(x, y, t) - \rho(x, y, \theta)c(x, y, \theta)\frac{\partial \theta}{\partial t} = 0, \quad (1)$$

where $Q(x, y, t)$ is the rate at which energy is generated per unit volume of the plate material, $\rho(x, y, \theta)$ and $c(x, y, \theta)$ are, respectively, the material mass density and specific heat, and $k_x(x, y, \theta)$ and $k_y(x, y, \theta)$ are the material heat transfer coefficients in directions x and y, respectively.

It should be recalled that the resolution of Eq. (1) must satisfy a set of initial and boundary conditions. Fig. 1 indicates that these later can be of two different categories, namely: enforcement of temperature values, $\theta(x, y, t) = \bar{\theta}(x, y, t)$ (a Dirichlet boundary condition), and enforcement of the heat flux in the direction normal to the contour line, $-q_n(x, y, t) = \bar{q}(x, y, t)$ (a Neumann boundary condition).

The complicating factors involved in Eq. (1) are material heterogeneity and anisotropy (i.e., material properties depend on direction and space coordinates) and non-linearity (material properties depend on the unknown temperature distribution). In addition, the arbitrary shape of the plate, which defines the domain to be covered by the solution.

Hence, a complicated problem such as this one can only be solved with recourse to numerical methods, among which, the FEM is a convenient one.

Currently, the Finite Element Method can be found implemented in a variety of commercial packages. Graphical interfaces are most often used, guiding the user across the different phases of modeling and numerical resolution. However, it is of utmost importance that the user fully understands the fundamentals of the method so as to be capable of making the appropriate modeling decisions and correctly interpreting results. In addition, there may be the need for the implementation of elements with particular characteristics, not available in the package's standard element library, and also the performance of the so-called *intrusive operations*. These later involve modifications of the FE model in its inner structure, as required in certain types of analyses, such as model adjustment to experimental data or system optimization. In such situations, mastering of physical, mathematical, numerical and computational aspects of the method is indispensable.

Therefore, in the subsection that follows, the basic steps involved in typical FE models are described aiming at, hopefully, providing the necessary understanding of how the method operates in commercial software and also helping the readers to implement their own code, should this be needed.

1.1 Fundamentals of the finite element method

Given the scope of the book to which this chapter belongs, an example focused on Solid Mechanics will be used for the description of the fundamental phases of FE modeling.

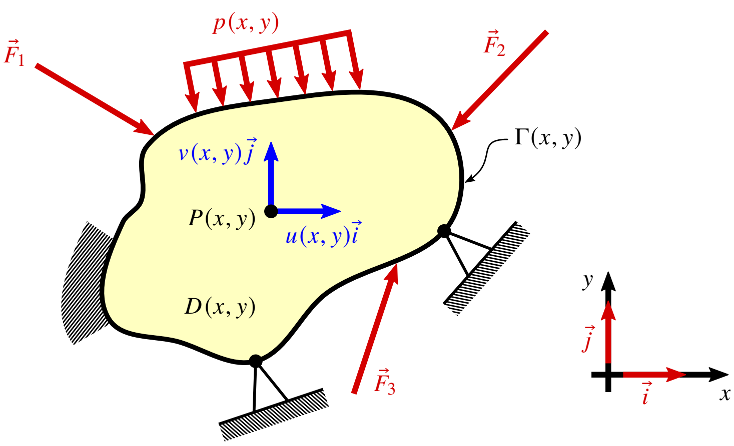

Figure 2: Illustration of a two-dimensional elasticity problem on a sheet of arbitrary shape.

Figure 2 illustrates a plane-stress elasticity problem, in which a thin sheet defining a domain $D(x, y)$ is subjected to in-plane loads, being constrained on a certain number of points on its boundary, which is indicated by $\Gamma(x, y)$. For simplicity, the assumptions of linear load-displacement material behavior and small displacements and rotations are adopted.

The classical problem to be solved consists in, given the loads and boundary conditions, determine the displacement Cartesian components $u(x, y)$ and $v(x, y)$ of each and every point $P(x, y)$ of the sheet, as well as the strain and stress distributions over the solid domain.

1.1.1 Spatial discretization of the domain

The first step of FE modeling is the division of the domain in which the problem is formulated (in the present example, the sheet and its boundary) in subdomains of predefined, user-selected, characteristics. These subdomains, called *elements*, are chosen to have simple geometry (triangles or quadrilaterals in two-dimensional problems; tetrahedrons or hexahedrons in three-dimensional problems), having given numbers of notable points, usually located on their edges, called *nodes*. Fig. 3 depicts the sheet of interest divided in a relatively large number of quadrilateral and triangular elements. Also shown is an amplified view of an element I, and its respective nodes,denoted by i, j, k, l. The entire set of elements and their nodes is named the model *mesh*.

Also indicated in Fig. 3 are the displacements of the four nodes of interest in directions x and y, denoted as $\vec{u}_i, \vec{v}_i, \vec{u}_j, \vec{v}_j, \vec{u}_k, \vec{v}_k, \vec{u}_l, \vec{v}_l$. In the finite element jargon, these displacements, or, more generally, the values of the unknown variables of the problem at the mesh nodes are called *degrees-of-freedom* (DOFs).

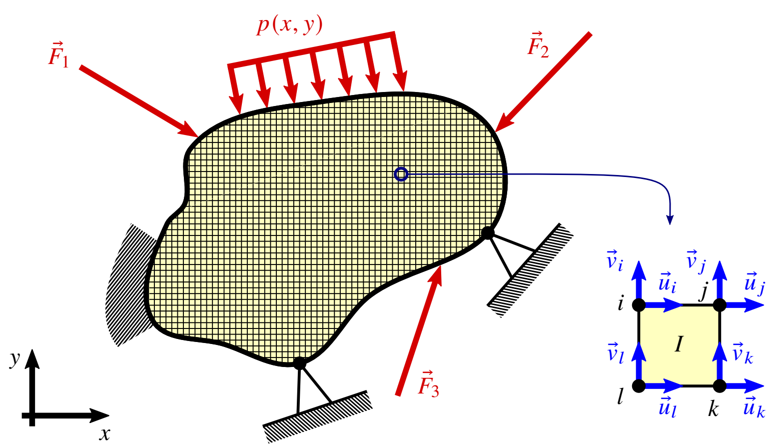

Figure 3: Illustration of a mesh defined for the discretization of a two-dimensional elasticity problem, and details of an element.

1.1.2 Interpolation of the field variables

Once defined the model mesh, the most distinguished idea underlying FE modeling is put forward, namely, the *interpolation* of the unknown variables, in the present case, the Cartesian components of the displacement field, *within each element of the mesh*. Accordingly, for a typical element I, these variables are mathematically expressed as follows:

$$u^{(I)}(x, y) = N_i(x, y)u_i + N_j(x, y)u_j + N_k(x, y)u_k + N_l(x, y)u_l, \tag{2a}$$

$$v^{(I)}(x, y) = N_i(x, y)v_i + N_j(x, y)v_j + N_k(x, y)v_k + N_l(x, y)v_l. \tag{2b}$$

It can be seen that, on each element, the displacement components at any point of coordinates (x, y) within the element, are expressed as linear combinations of the corresponding values evaluated at the four nodes. The coefficients of these linear combinations are the functions of the space coordinates $N_i(x, y), N_j(x, y), N_k(x, y), N_l(x, y)$. These functions, called *interpolation functions* or *shape functions*, are chosen for each particular type of element. In general, they are polynomial functions whose degrees are chosen according to the number of nodes (and DOFs, as a result) assigned to the elements.

It should be highlighted that, once the nodal values of the unknowns are determined, the values of the variables $u^{(I)}(x, y)$ and $v^{(I)}(x, y)$ are obtained as continuous functions of the nodal values, as given by Eqs. (2). Hence, the primary goal of finite element computations is the determination of the nodal values, the number of which is finite, as opposed to the number of variables in the original Solid Mechanics problem, governed by partial differential equations, whose solution over the entire domain $u(x, y), v(x, y)$ must be valid for the infinite number of points comprising the domain. It can, thus, be stated that the combination of the discretization and interpolation procedures enables to reduce the original infinite-dimensional problem to an associated finite-dimensional one, amenable to approximate numerical resolution. This entails transitions from one type of mathematical model (for the continuous problem) to another (for the discretized problem). For example, in the case of transient heat transfer problems, the transition leads from a partial differential equation to a set of (generally coupled) ordinary differential equations having the nodal temperature values as unknowns; in the case of equilibrium problems of elasticity, the transition is made from a set of partial differential equations to a set of coupled algebraic equations having the nodal displacement values as unknowns.

1.1.3 Formulation at element level

The formulation at the so-called *element level* is carried-out by considering the physics of the problem, starting either from basic governing principles or, more directly, the differential equations governing the underlying phenomena. For this purpose, three different formulation approaches can be followed, which are described next. Irrespective of the approach adopted, the goal is to establish differential or algebraic relations between inputs applied at the element nodes, and resulting outputs at the nodes. For example, in heat transfer problems, the inputs are heat fluxes and the outputs are temperatures; in static elasticity problems, the inputs are forces and the outputs are displacements. At this level, each element is considered individually, without any interaction with neighboring elements.

- **Direct approach:** in this approach, the equations describing the underlying principles are directly manipulated, in association with interpolation of the field variables to obtain the above-mentioned input-output relations. As examples, in heat transfer problems, energy balance and Fourier's law are jointly used with interpolated temperature field within the element to obtain relations between heat fluxes applied at the nodes and the corresponding nodal temperature values; in static elasticity problems, equilibrium equations and material constitutive laws, together with interpolated displacement fields lead to relations between forces applied at the nodes and the associated nodal displacement values. In spite of providing clear physical meaning of the operations performed during the derivation of the input-output relations at the element level, the direct approach is mostly used in the formulation of one-dimensional problems, since its extension to two- or three-dimensional problems tend to involve rather cumbersome manipulations.

- **Variational approach:** this approach is based on the exploration of the so-called *variational principles*, which establish stationarity conditions to be satisfied by certain functionals that, in many cases, are integrals expressing the energy of the system. From the mathematical standpoint, methods for finding the extremals of such functionals are in the scope of a branch of Mathematics known as Variational Calculus [Weinstock, 1975, Lanczos, 1986]. In the case of mechanical systems of interest here, the most widely used variational principles are the *Principle of Minimal Potential Energy*, which, applied to elastic systems, states that, among all possible deformed configurations satisfying the prescribed boundary conditions, the actual configuration developed is the one that minimizes the total potential energy of the system; and the *Hamilton's Variational Principle*, which establishes that, for dynamic systems, the actual motion evolution, satisfying boundary and initial conditions, must extremize a functional expressing the net value of the difference between the kinetic and potential energies.

For the variational formulation at element level, the applicable variational principle is used in combination with the interpolation of field variables and, searching the conditions to be satisfied by the aproximate solution to ensure the stationarity of the associated functional. Eventually, the stationarity conditions are brought to the requirement that the derivatives of the algebraic form of functional with respect to each DOF of the element must vanish. This procedure leads to the input-output relations at element level that are searched for.

In spite of being very powerful and elegant, the use of the variational approach is confined to problems governed by variational principles, which is not always the case.

- **Weighted residuals approach**: this approach operates directly on the differential equations governing the problem into consideration. The main idea is to establish the conditions to be satisfied by the approximated solution in such a way to minimize the solution errors expressed as mean values of point-wise weighted residual functions, evaluated over an individual element. The number of errors considered is equal to the number of DOFs of the element, and each one is obtained from a different weighting function.

  The computation of the errors involve the integration of the corresponding weighted residual functions over the element. The use of Gauss' Theorem or Green's Theorem (according to the dimensionality of the problem) enables one to reduce the maximal order of the differential operators in the integrand, leading to the so-called *weak form* of the problem.

  Various weight residual methods have been devised, making use of different weighting functions. Among them, the most popular (at least in the scope of FE modeling) is the *Galerkin Method*, in which the shape functions are used as weighting functions.

  Similarly to the two previous formulation approaches, the weight residual approach eventually leads to the searched input-output relations at element level.

1.1.4 Formulation at global level

In the formulation at element level, each element of the mesh is considered individually, without any physical interaction among them. This means that, at that level, the formulation leads to a set of uncoupled equations expressing the input-output relations for each and every element of the mesh. However, as can be seen in Fig. 3, all the elements of the mesh will have at least one neighboring element with which it shares nodes and DOFs. This means, from the physics perspective, that at nodes shared by neighboring elements, the continuity of the field variables must be ensured, as well as other requirements depending of the specific nature of the problem, such as force equilibrium and null net heat flux. These conditions are enforced by appropriate modification and combination of the input-output relations previously established for each element at element level, which leads to relations between outputs and inputs at global level, represented, respectively by vectors containing the whole set of nodal DOFs and nodal loads. These two vectors are related to each other by a square multiplicative matrix (known as *global stiffness matrix* in Solid Mechanics problems.

From the algorithmic standpoint, enforcement of the above-mentioned conditions is made by a sequence of well-defined matrix operations, known as *matrix/vector assembling* [Zienkiewicz et al., 2013, Reddy, 2019].

1.1.5 Enforcement of boundary conditions

Upon completion of matrix/vector assembling, the input-output relations for the whole FE model are available, nonetheless without any constraints imposed to the DOFs. Hence, the global matrices and vectors must be further modified to account for the boundary conditions. In Solid Mechanics problems, for example, very often those conditions represent specific values assigned to particular DOFs associated to nodes located on the boundary of the body.

1.1.6 Numerical resolution

The finite element equations at global level have to be solved by using appropriate numerical procedures. According to the nature of the problem, different types of equations must be solved: for equilibrium or steady-state problems, one has systems of algebraic equations, while for dynamic or transient problems, systems of ordinary differential equations are to be solved. Furthermore, within these broad categories of problems, some specific numerical problems may emerge. For example, static or dynamic stability problems require the resolution of *eigenvalue problems*, while the frequency response analysis in structural dynamics require the resolution of a series of sets of linear algebraic equations, each one corresponding to a discrete value of frequency.

In addition to the calculation of the primary unknowns of the FE model, by the resolution of the equations mentioned above, further computations are required to determine other quantities derived from those unknowns. As an example, in linear elasticity problems, most often the primary unknowns are the nodal displacements. In these cases, strain distributions must be determined by applying the appropriate differential operators to the displacement distributions at element level, according to the strain-displacement relations. Then, stress distributions are computed by making recourse to the stress-strain relations at element level, which involve the matrix of elastic parameters. These additional computations are most-often referred to as *post-processing* of the primary solution of the underlying problem.

At this point it is important to point-out that the efficiency of the FE method highly depends on the efficiency of the numerical algorithms used for the resolution of the different types of mathematical equations mentioned above. This is due to the fact that, to provide the necessary accuracy, complex finite element models must use highly refined discretization meshes, which leads to large numbers of DOFs and numbers of equations to be solved simultaneously (of the order of 10^5 to 10^7). In addition, in the majority of applications of practical interest (model updating based on experimental data, structural optimization, uncertainty propagation, etc.) the numerical resolution of the mathematical equations must be made multiple times. As a result, computational burden tend to be typically high and must be properly managed to render the computations feasible for the computer resources available. Besides the search for increasingly efficient numerical methods, the alleviation of computation cost can be achieved by employing techniques of model condensation and metamodeling [Zu-Qing, 2004, Gratiet et al., 2017, Sargsyan, 2017, Chen and Schwab, 2017].

2 Modeling of Problems in Solid Mechanics (Variational Approach)

The application and formulation of the FEM for problems in Solid Mechanics can be carried out using various strategies, as briefly explained in the previous section. Here, the variational approach is adopted, due to its versatility and relatively simple background requirements. While previous knowledge on Variational Calculus should not be required to follow the developments presented next, the reader can consult other material available on the matter if he/she has desire to do so [Weinstock, 1975, Lanczos, 1986].

Additionally, one assumes the reader to be reasonably familiar with Solid Mechanics. Various concepts invoked in the sequence can be found in more specific literature, e.g. [Fung et al., 2017].

Within the framework of the variational formulation of the FEM, one seeks to make a functional stationary. In the case of structural dynamics problems, such functional is directly related to the Lagrangian, $\mathcal{L}$, given by the difference between kinetic $\mathcal{K}$ and potential $\mathcal{U}$ energies:

$$\mathcal{L} = \mathcal{K} - \mathcal{U}. \tag{3}$$

Both contributions arise due to the motion of a solid body. Referring to Fig. 4, let us denote the velocities of an arbitrary point by $\dot{u}(x, y, z, t)$, $\dot{v}(x, y, z, t)$ and $\dot{w}(x, y, z, t)$ along the three Cartesian coordinate directions, where $\dot{(\ )} \equiv \mathrm{d}(\ )/\mathrm{d}t$. The kinetic energy of the solid body can therefore be obtained by:

$$\mathcal{K}(t) = \iiint_{\Omega_t} \frac{1}{2}\rho(x, y, z) \left[\dot{u}^2(x, y, z, t) + \dot{v}^2(x, y, z, t) + \dot{w}^2(x, y, z, t)\right] \mathrm{d}x\,\mathrm{d}y\,\mathrm{d}z, \tag{4}$$

where ρ denotes the mass density, and Ω_t the volume occupied by the body at time t. In essence, the previous equation is the continuum counterpart of that one related to a collection of discrete particles; it can be interpreted as the (Riemann) sum of half the mass times the square of the velocity magnitude of each continuum (differential) particle.

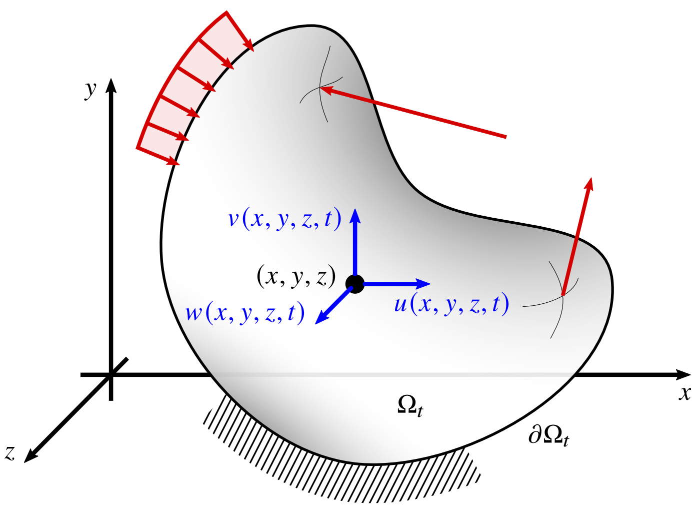

Figure 4: Snapshot of a solid body during its motion, at time t, with volume Ω_t and boundary $\partial\Omega_t$.

With regards to the potential energy, it can encompass various contributions (due to elasticity, gravity, ...), but all being related to conservative loads, i.e. those whose mechanical work do not depend on the load-path. Considering that the theory of elasticity holds (i.e. small/infinitesimal displacements and strains are assumed), $\mathcal{U}$ can be obtained using:

$$\mathcal{U}(t) = \frac{1}{2} \iiint_{\Omega_t} \left[\sigma_x \epsilon_x + \sigma_y \epsilon_y + \sigma_z \epsilon_z + \tau_{xy}\gamma_{xy} + \tau_{xz}\gamma_{xz} + \tau_{yz}\gamma_{yz}\right] \mathrm{d}x\, \mathrm{d}y\, \mathrm{d}z - \mathcal{W}_{\mathrm{ext}}, \tag{5}$$

where $\sigma_i = \sigma_i(x, y, z, t)$ and $\tau_{ij} = \tau_{ij}(x, y, z, t)$ $(i, j \in \{x, y, z\})$ stand for the Cartesian components of the engineering stress tensor; and $\epsilon_i = \epsilon_i(x, y, z, t)$ and $\gamma_{ij} = 2\epsilon_{ij} = \gamma_{ij}(x, y, z, t)$ $(i, j \in \{x, y, z\})$ represent the Cartesian components of the infinitesimal strain tensor and shear angles, respectively. Additionally, $\mathcal{W}_{\mathrm{ext}}$ represents the work done by conservative external forces. It can be calculated, in general, according to:

$$\begin{aligned}\mathcal{W}_{\mathrm{ext}}(t) = \iiint_{\Omega_t} & \left[u(x, y, z, t) f_b^x(x, y, z, t) + v(x, y, z, t) f_b^y(x, y, z, t)\right. \\ & \left. + w(x, y, z, t) f_b^z(x, y, z, t)\right] \mathrm{d}x\, \mathrm{d}y\, \mathrm{d}z \\ + \iint_{\partial\Omega_t} & \left[u(x, y, z, t) f_s^x(x, y, z, t) + v(x, y, z, t) f_s^y(x, y, z, t)\right. \\ & \left. + w(x, y, z, t) f_s^z(x, y, z, t)\right] \mathrm{d}S,\end{aligned} \tag{6}$$

where f_b^x, f_b^y and f_b^z represent body forces (forces per unit volume, such as the one due to gravity) and f_s^x, f_s^y and f_s^s correspond to surface forces (forces per unit area, e.g. tractions, pressures, concentrated loads). The boundary of the body, on which surface forces can be applied, is denoted $\partial\Omega_t$, and $\mathrm{d}S$ represents a differential area/surface element.

Additional equations need to be taken into account to allow for specification of the solid's material behavior. These equations are known as constitutive equations. If the solid behavior is in accordance with linear elasticity, and its properties are the same in every direction (i.e. the material is isotropic), then its constitutive equations correspond to Hooke's law. In the case of three-dimensional elasticity, it reads:

$$\sigma_x = \tfrac{E}{(1+\nu)(1-2\nu)} \left[(1-\nu)\epsilon_x - \nu\epsilon_y - \nu\epsilon_z\right]; \tag{7a}$$

$$\sigma_y = \tfrac{E}{(1+\nu)(1-2\nu)} \left[-\nu\epsilon_x + (1-\nu)\epsilon_y - \nu\epsilon_z\right]; \tag{7b}$$

$$\sigma_z = \tfrac{E}{(1+\nu)(1-2\nu)} \left[-\nu\epsilon_x - \nu\epsilon_y + (1-\nu)\epsilon_z\right]; \tag{7c}$$

$$\tau_{xy} = G\gamma_{xy}; \tag{7d}$$

$$\tau_{xz} = G\gamma_{xz}; \tag{7e}$$

$$\tau_{yz} = G\gamma_{yz}, \tag{7f}$$

with E, ν and $G = E/[2(1+\nu)]$ corresponding to the material's Young's modulus, Poisson's ratio and shear modulus, respectively. Of course, more general constitutive relations can be considered, depending on the material one wants to model.

Other important equations which need to be recalled relate strains to the displacements experienced by the solid body during its motion. From the theory of linear elasticity, the following holds:

$$\epsilon_x = \frac{\partial u}{\partial x}; \quad \epsilon_y = \frac{\partial v}{\partial y}; \quad \epsilon_z = \frac{\partial w}{\partial z}; \quad \gamma_{xy} = \frac{\partial u}{\partial y} + \frac{\partial v}{\partial x}; \quad \gamma_{xz} = \frac{\partial u}{\partial z} + \frac{\partial w}{\partial x}; \quad \gamma_{yz} = \frac{\partial v}{\partial z} + \frac{\partial w}{\partial y}, \tag{8}$$

where dependencies have been omitted for conciseness.

As discussed in section 1 of this chapter, within the context of the FEM, the continuum solid body is replaced by a mesh, formed by finite elements and their respective nodes. In this process, the unknown displacement fields u, v and w have their spatial dependency become expressed in terms of nodal DOFs. In this sense, inside the domain of a given finite element, the displacement fields are interpolated (approximated) based on the nodal DOFs. Mathematically, for a generic element e of the mesh, we have, akin to Eqs. (2), for example:

$$u^{(e)}(x, y, z, t) = \sum_{k=1}^{n^{(e)}} N_{uk}^{(e)}(x, y, z)q_k^{(e)}(t) = \mathbf{N}_u^{(e)}(x, y, z)\mathbf{q}^{(e)}(t); \tag{9a}$$

$$v^{(e)}(x, y, z, t) = \sum_{k=1}^{n^{(e)}} N_{vk}^{(e)}(x, y, z)q_k^{(e)}(t) = \mathbf{N}_v^{(e)}(x, y, z)\mathbf{q}^{(e)}(t); \tag{9b}$$

$$w^{(e)}(x, y, z, t) = \sum_{k=1}^{n^{(e)}} N_{wk}^{(e)}(x, y, z)q_k^{(e)}(t) = \mathbf{N}_w^{(e)}(x, y, z)\mathbf{q}^{(e)}(t), \tag{9c}$$

where the vector $\mathbf{q}^{(e)}(t) \in \mathbb{R}^{n^{(e)}\times 1}$ collects the element nodal DOFs, in a total of $n^{(e)}$. These could comprise, for instance, the displacements of the nodes. Matrices such as $\mathbf{N}_u^{(e)}(x, y, z)$, $\mathbf{N}_v^{(e)}(x, y, z)$ and $\mathbf{N}_v^{(e)}(x, y, z)$, of size $1 \times n^{(e)}$, contain the so-called *interpolation functions* or *shape functions* of the finite element. They enable us to compute the displacements of any point within the finite element domain in terms of its nodal DOFs, after these have been obtained.

An important note in this regard is that each type of finite element has its own particular set of interpolation functions. Hence, the choice of a finite element to be used in a particular analysis directly translates to which interpolation functions are used. This is important to be recognized because the interpolation functions can hinder its corresponding finite element from adequately representing certain behaviors. This is another reason for which it is of utmost significance for one to become aware of the formulation of the FEM, as well as of documentation and/or manuals of various commercial finite element packages.

Traditionally, in the formulation of finite elements, interpolation functions are chosen to be polynomials, although this is not the only option, nor necessarily the better. For instance, non-uniform rational B-splines (NURBS) can be used, as considered in the so-called isogeometric finite element analysis [Cottrell et al., 2009].

In the following, instead of presenting the mathematical formulation of a finite element method for three-dimensional elasticity, we favor the case of two-dimensional elasticity. A finite element for the more complicated case can be obtained following similar steps to those outlined next.

2.1 Quadrilateral finite element for two-dimensional elasticity problems

2.1.1 Element geometry and interpolation of field variables

The two-dimensional elasticity finite element we consider here has four nodes, and its geometry is quadrilateral, cf. Fig. 5.

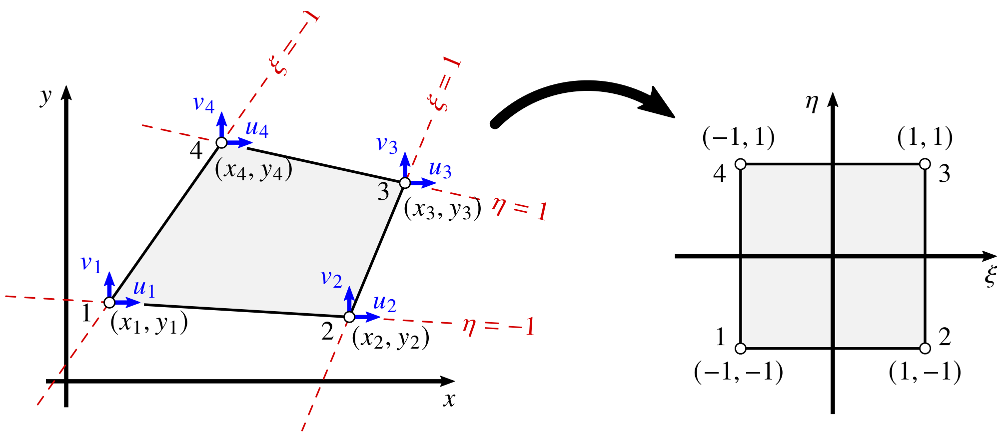

Figure 5: Geometry of a quadrilateral finite element with four nodes, and its corresponding representation in the natural coordinate space (ξ, η).

The degrees of freedom of the element are chosen to correspond to the displacements at the nodes. In this way, we have:

$$\mathbf{q}^{(e)}(t) = \begin{Bmatrix} u_1(t) & v_1(t) & u_2(t) & v_2(t) & u_3(t) & v_3(t) & u_4(t) & v_4(t) \end{Bmatrix}^{\mathrm{T}}, \tag{10}$$

in which $u_i(t)$, $v_i(t)$ correspond to the displacements of node i along the x and y directions, respectively. At this stage, we drop the superscript $^{(e)}$ to avoid clutter – it will be used again later when needed to avoid possible confusion.

Having this at hand, we must select an interpolation scheme for evaluating the displacement fields inside the element domain. For this purpose, we choose the following polynomials:

$$u(x,y,t) = a_{00}(t) + a_{10}(t)x + a_{01}(t)y + a_{11}(t)xy = \begin{bmatrix} 1 & x & y & xy \end{bmatrix} \begin{Bmatrix} a_{00}(t) \\ a_{10}(t) \\ a_{01}(t) \\ a_{11}(t) \end{Bmatrix}; \tag{11a}$$

$$v(x,y,t) = b_{00}(t) + b_{10}(t)x + b_{01}(t)y + b_{11}(t)xy = \begin{bmatrix} 1 & x & y & xy \end{bmatrix} \begin{Bmatrix} b_{00}(t) \\ b_{10}(t) \\ b_{01}(t) \\ b_{11}(t) \end{Bmatrix}, \tag{11b}$$

for any $(x,y) \in \Omega_t^{(e)}$. The time-dependent weights a_{ij}, b_{ij} $(i,j \in \{0,1\})$ can be determined by enforcing the value of the displacement fields at the element nodes, i.e.,

$$\begin{Bmatrix} u_1(t) \\ u_2(t) \\ u_3(t) \\ u_4(t) \end{Bmatrix} = \begin{Bmatrix} u(x_1,y_1,t) \\ u(x_2,y_2,t) \\ u(x_3,y_3,t) \\ u(x_4,y_4,t) \end{Bmatrix} = \begin{bmatrix} 1 & x_1 & y_1 & x_1y_1 \\ 1 & x_2 & y_2 & x_2y_2 \\ 1 & x_3 & y_3 & x_3y_3 \\ 1 & x_4 & y_4 & x_4y_4 \end{bmatrix} \begin{Bmatrix} a_{00}(t) \\ a_{10}(t) \\ a_{01}(t) \\ a_{11}(t) \end{Bmatrix} \Rightarrow$$

$$\Rightarrow \begin{Bmatrix} a_{00}(t) \\ a_{10}(t) \\ a_{01}(t) \\ a_{11}(t) \end{Bmatrix} = \begin{bmatrix} 1 & x_1 & y_1 & x_1y_1 \\ 1 & x_2 & y_2 & x_2y_2 \\ 1 & x_3 & y_3 & x_3y_3 \\ 1 & x_4 & y_4 & x_4y_4 \end{bmatrix}^{-1} \begin{Bmatrix} u_1(t) \\ u_2(t) \\ u_3(t) \\ u_4(t) \end{Bmatrix}; \tag{12a}$$

$$\begin{Bmatrix} v_1(t) \\ v_2(t) \\ v_3(t) \\ v_4(t) \end{Bmatrix} = \begin{Bmatrix} v(x_1,y_1,t) \\ v(x_2,y_2,t) \\ v(x_3,y_3,t) \\ v(x_4,y_4,t) \end{Bmatrix} = \begin{bmatrix} 1 & x_1 & y_1 & x_1y_1 \\ 1 & x_2 & y_2 & x_2y_2 \\ 1 & x_3 & y_3 & x_3y_3 \\ 1 & x_4 & y_4 & x_4y_4 \end{bmatrix} \begin{Bmatrix} b_{00}(t) \\ b_{10}(t) \\ b_{01}(t) \\ b_{11}(t) \end{Bmatrix} \Rightarrow$$

$$\Rightarrow \begin{Bmatrix} b_{00}(t) \\ b_{10}(t) \\ b_{01}(t) \\ b_{11}(t) \end{Bmatrix} = \begin{bmatrix} 1 & x_1 & y_1 & x_1y_1 \\ 1 & x_2 & y_2 & x_2y_2 \\ 1 & x_3 & y_3 & x_3y_3 \\ 1 & x_4 & y_4 & x_4y_4 \end{bmatrix}^{-1} \begin{Bmatrix} v_1(t) \\ v_2(t) \\ v_3(t) \\ v_4(t) \end{Bmatrix}. \tag{12b}$$

Combining these results with Eq. (11), we obtain:

$$\begin{aligned} u(x,y,t) &= \begin{bmatrix} 1 & x & y & xy \end{bmatrix} \begin{Bmatrix} a_{00}(t) \\ a_{10}(t) \\ a_{01}(t) \\ a_{11}(t) \end{Bmatrix} = \begin{bmatrix} 1 & x & y & xy \end{bmatrix} \begin{bmatrix} 1 & x_1 & y_1 & x_1y_1 \\ 1 & x_2 & y_2 & x_2y_2 \\ 1 & x_3 & y_3 & x_3y_3 \\ 1 & x_4 & y_4 & x_4y_4 \end{bmatrix}^{-1} \begin{Bmatrix} u_1 \\ u_2 \\ u_3 \\ u_4 \end{Bmatrix} \\ &= N_1(x,y)u_1(t) + N_2(x,y)u_2(t) + N_3(x,y)u_3(t) + N_4(x,y)u_4(t); \end{aligned} \tag{13a}$$

$$v(x,y,t) = \begin{bmatrix} 1 & x & y & xy \end{bmatrix} \begin{Bmatrix} b_{00}(t) \\ b_{10}(t) \\ b_{01}(t) \\ b_{11}(t) \end{Bmatrix} = \begin{bmatrix} 1 & x & y & xy \end{bmatrix} \begin{bmatrix} 1 & x_1 & y_1 & x_1y_1 \\ 1 & x_2 & y_2 & x_2y_2 \\ 1 & x_3 & y_3 & x_3y_3 \\ 1 & x_4 & y_4 & x_4y_4 \end{bmatrix}^{-1} \begin{Bmatrix} v_1 \\ v_2 \\ v_3 \\ v_4 \end{Bmatrix}$$

$$= N_1(x,y)v_1(t) + N_2(x,y)v_2(t) + N_3(x,y)v_3(t) + N_4(x,y)v_4(t), \tag{13b}$$

from which the expressions for $N_i(x,y)$ ($i \in \{1,2,3,4\}$) can be identified. While the expressions for these shape functions can be established analytically (using symbolic algebra software, for example), they result relatively complicated and long, being for this reason omitted here.

It is sometimes more convenient in the formulation of finite elements to adopt a different strategy, which relies on the use of a natural coordinate system (ξ,η), instead of the Cartesian (x,y) one. In this setting, the positions of the nodes of a finite element assume normalized values, as can be seen in Fig. 5. Using the natural coordinate system, we can write:

$$u(\xi,\eta,t) = \begin{bmatrix} 1 & \xi & \eta & \xi\eta \end{bmatrix} \begin{bmatrix} 1 & \xi_1 & \eta_1 & \xi_1\eta_1 \\ 1 & \xi_2 & \eta_2 & \xi_2\eta_2 \\ 1 & \xi_3 & \eta_3 & \xi_3\eta_3 \\ 1 & \xi_4 & \eta_4 & \xi_4\eta_4 \end{bmatrix}^{-1} \begin{Bmatrix} u_1(t) \\ u_2(t) \\ u_3(t) \\ u_4(t) \end{Bmatrix}$$

$$= N_1(\xi,\eta)u_1(t) + N_2(\xi,\eta)u_2(t) + N_3(\xi,\eta)u_3(t) + N_4(\xi,\eta)u_4(t); \tag{14a}$$

$$v(\xi,\eta,t) = \begin{bmatrix} 1 & \xi & \eta & \xi\eta \end{bmatrix} \begin{bmatrix} 1 & \xi_1 & \eta_1 & \xi_1\eta_1 \\ 1 & \xi_2 & \eta_2 & \xi_2\eta_2 \\ 1 & \xi_3 & \eta_3 & \xi_3\eta_3 \\ 1 & \xi_4 & \eta_4 & \xi_4\eta_4 \end{bmatrix}^{-1} \begin{Bmatrix} v_1(t) \\ v_2(t) \\ v_3(t) \\ v_4(t) \end{Bmatrix}$$

$$= N_1(\xi,\eta)v_1(t) + N_2(\xi,\eta)v_2(t) + N_3(\xi,\eta)v_3(t) + N_4(\xi,\eta)v_4(t), \tag{14b}$$

where now it is easy to express $N_i(\xi,\eta)$ ($i \in \{1,2,3,4\}$):

$$N_1(\xi,\eta) = \tfrac{1}{4}(1-\xi)(1-\eta); \qquad N_2(\xi,\eta) = \tfrac{1}{4}(1+\xi)(1-\eta);$$

$$N_3(\xi,\eta) = \tfrac{1}{4}(1+\xi)(1+\eta); \qquad N_4(\xi,\eta) = \tfrac{1}{4}(1-\xi)(1+\eta). \tag{15}$$

We should note, at this stage, that the position of an arbitrary point on the domain of a given finite element (of the considered type) can be obtained using the same interpolation functions presented above, i.e.

$$x(\xi,\eta) = N_1(\xi,\eta)x_1 + N_2(\xi,\eta)x_2 + N_3(\xi,\eta)x_3 + N_4(\xi,\eta)x_4; \tag{16a}$$

$$y(\xi,\eta) = N_1(\xi,\eta)y_1 + N_2(\xi,\eta)y_2 + N_3(\xi,\eta)y_3 + N_4(\xi,\eta)y_4. \tag{16b}$$

Finite elements for which the same functions are used to interpolate the coordinates of a point on the element domain and unknown field variables (such as u and v in our presentation) are known as *isoparametric* finite elements [Bathe, 2014, Zienkiewicz et al., 2013].

As will be shown in developments which will follow soon, functions which depend on $N_i(x,y)$, as well as on their spatial derivatives, will need to be integrated on the domain of a finite element – so that relevant structural matrices can be obtained. Since one has favored the use of a natural coordinate system, we must be able to perform coordinate transformation between (x,y) and (ξ,η). By employing the chain-rule of differentiation:

$$\begin{cases} x = x(\xi,\eta) \\ y = y(\xi,\eta) \end{cases} \quad \Rightarrow \quad \begin{Bmatrix} \dfrac{\partial(\cdot)}{\partial\xi} \\ \dfrac{\partial(\cdot)}{\partial\eta} \end{Bmatrix} = \begin{bmatrix} \dfrac{\partial x}{\partial\xi} & \dfrac{\partial y}{\partial\xi} \\ \dfrac{\partial x}{\partial\eta} & \dfrac{\partial y}{\partial\eta} \end{bmatrix} \begin{Bmatrix} \dfrac{\partial(\cdot)}{\partial x} \\ \dfrac{\partial(\cdot)}{\partial y} \end{Bmatrix}$$

$$\text{and} \quad \begin{Bmatrix} \dfrac{\partial(\cdot)}{\partial x} \\ \dfrac{\partial(\cdot)}{\partial y} \end{Bmatrix} = \begin{bmatrix} \dfrac{\partial x}{\partial\xi} & \dfrac{\partial y}{\partial\xi} \\ \dfrac{\partial x}{\partial\eta} & \dfrac{\partial y}{\partial\eta} \end{bmatrix}^{-1} \begin{Bmatrix} \dfrac{\partial(\cdot)}{\partial\xi} \\ \dfrac{\partial(\cdot)}{\partial\eta} \end{Bmatrix}, \tag{17}$$

based on which we define the Jacobian matrix related to an element:

$$\mathbf{J} = \begin{bmatrix} \dfrac{\partial x}{\partial \xi} & \dfrac{\partial y}{\partial \xi} \\ \dfrac{\partial x}{\partial \eta} & \dfrac{\partial y}{\partial \eta} \end{bmatrix}, \tag{18}$$

whose entries, from Eqs. (15) and (16), can be obtained as:

$$J_{11} = \frac{\partial x}{\partial \xi} = -\frac{1}{4}(1-\eta)\,x_1 + \frac{1}{4}(1-\eta)\,x_2 + \frac{1}{4}(1+\eta)\,x_3 - \frac{1}{4}(1+\eta)\,x_4; \tag{19a}$$

$$J_{12} = \frac{\partial y}{\partial \xi} = -\frac{1}{4}(1-\eta)\,y_1 + \frac{1}{4}(1-\eta)\,y_2 + \frac{1}{4}(1+\eta)\,y_3 - \frac{1}{4}(1+\eta)\,y_4; \tag{19b}$$

$$J_{21} = \frac{\partial x}{\partial \eta} = -\frac{1}{4}(1-\xi)\,x_1 - \frac{1}{4}(1+\xi)\,x_2 + \frac{1}{4}(1+\xi)\,x_3 + \frac{1}{4}(1-\xi)\,x_4; \tag{19c}$$

$$J_{22} = \frac{\partial y}{\partial \eta} = -\frac{1}{4}(1-\xi)\,y_1 - \frac{1}{4}(1+\xi)\,y_2 + \frac{1}{4}(1+\xi)\,y_3 + \frac{1}{4}(1-\xi)\,y_4. \tag{19d}$$

Having in mind the expression put forward for $\mathbf{q}^{(e)}(t)$, cf. Eq. (10), we can see that:

$$\begin{aligned} u^{(e)}(\xi,\eta,t) &= \mathbf{N}_u^{(e)}(\xi,\eta)\mathbf{q}^{(e)}(t) \\ &= \begin{bmatrix} N_1(\xi,\eta) & 0 & N_2(\xi,\eta) & 0 & N_3(\xi,\eta) & 0 & N_4(\xi,\eta) & 0 \end{bmatrix} \mathbf{q}^{(e)}(t); \end{aligned} \tag{20a}$$

$$\begin{aligned} v^{(e)}(\xi,\eta,t) &= \mathbf{N}_v^{(e)}(\xi,\eta)\mathbf{q}^{(e)}(t) \\ &= \begin{bmatrix} 0 & N_1(\xi,\eta) & 0 & N_2(\xi,\eta) & 0 & N_3(\xi,\eta) & 0 & N_4(\xi,\eta) \end{bmatrix} \mathbf{q}^{(e)}(t). \end{aligned} \tag{20b}$$

2.1.2 Formulation at element level

Having established the interpolation of the field variables of the problem at hand, now one aims toward obtaining expressions for the Lagrangian of an element, directly involving its nodal DOFs. After the Lagrangian is obtained, it can established the dynamic equilibrium equations which one seeks here, based on the stationarity of the relevant functional.

For this, firstly, interpolation relations for the relevant strains are derived. By combining Eqs. (8) and (20), it is possible to arrive at:

$$\epsilon_x^{(e)}(\xi,\eta,t) = \frac{\partial u^{(e)}}{\partial x} = \frac{\partial \mathbf{N}_u^{(e)}(\xi,\eta)}{\partial x}\mathbf{q}^{(e)}(t) = \mathbf{B}_x^{(e)}(\xi,\eta)\mathbf{q}^{(e)}(t); \tag{21a}$$

$$\epsilon_y^{(e)}(\xi,\eta,t) = \frac{\partial v^{(e)}}{\partial y} = \frac{\partial \mathbf{N}_v^{(e)}(\xi,\eta)}{\partial y}\mathbf{q}^{(e)}(t) = \mathbf{B}_y^{(e)}(\xi,\eta)\mathbf{q}^{(e)}(t); \tag{21b}$$

$$\gamma_{xy}^{(e)}(\xi,\eta,t) = \frac{\partial u^{(e)}}{\partial y} + \frac{\partial v^{(e)}}{\partial x} = \frac{\partial \mathbf{N}_u^{(e)}(\xi,\eta)}{\partial y}\mathbf{q}^{(e)}(t) + \frac{\partial \mathbf{N}_v^{(e)}(\xi,\eta)}{\partial x}\mathbf{q}^{(e)}(t) = \mathbf{B}_{xy}^{(e)}(\xi,\eta)\mathbf{q}^{(e)}(t). \tag{21c}$$

By invoking Eq. (17), explicit expressions can be established for the strain interpolation matrices, if so desired:

$$\mathbf{B}_x^{(e)} = \frac{1}{8\det\mathbf{J}^{(e)}}\begin{bmatrix} (1-\eta)y_2 - (\xi-\eta)y_3 - (1-\xi)y_4 \\ 0 \\ -(1-\eta)y_1 + (1+\xi)y_3 - (\xi+\eta)y_4 \\ 0 \\ (\xi-\eta)y_1 - (1+\xi)y_2 + (1+\eta)y_4 \\ 0 \\ (1-\xi)y_1 + (\xi+\eta)y_2 - (1+\eta)y_3 \\ 0 \end{bmatrix}^{\mathrm{T}}; \tag{22a}$$

$$\mathbf{B}_y^{(e)} = \frac{1}{8\det\mathbf{J}^{(e)}}\begin{bmatrix} 0 \\ -(1-\eta)x_2 + (\xi-\eta)x_3 + (1-\xi)x_4 \\ 0 \\ (1-\eta)x_1 - (1+\xi)x_3 + (\xi+\eta)x_4 \\ 0 \\ -(\xi-\eta)x_1 + (1+\xi)x_2 - (1+\eta)x_4 \\ 0 \\ -(1-\xi)x_1 - (\xi+\eta)x_2 + (1+\eta)x_3 \end{bmatrix}^{\mathrm{T}}; \tag{22b}$$

$$\mathbf{B}_{xy}^{(e)} = \frac{1}{8\det\mathbf{J}^{(e)}}\begin{bmatrix} -(1-\eta)x_2 + (\xi-\eta)x_3 + (1-\xi)x_4 \\ (1-\eta)y_2 - (\xi-\eta)y_3 - (1-\xi)y_4 \\ (1-\eta)x_1 - (1+\xi)x_3 + (\xi+\eta)x_4 \\ -(1-\eta)y_1 + (1+\xi)y_3 - (\xi+\eta)y_4 \\ -(\xi-\eta)x_1 + (1+\xi)x_2 - (1+\eta)x_4 \\ (\xi-\eta)y_1 - (1+\xi)y_2 + (1+\eta)y_4 \\ -(1-\xi)x_1 - (\xi+\eta)x_2 + (1+\eta)x_3 \\ (1-\xi)y_1 + (\xi+\eta)y_2 - (1+\eta)y_3 \end{bmatrix}^{\mathrm{T}}, \tag{22c}$$

where $\det\mathbf{J}^{(e)} = J_{11}^{(e)}J_{22}^{(e)} - J_{12}^{(e)}J_{21}^{(e)}$.

Now, to facilitate manipulations, it is more convenient to arrange the strains in a single vector, as follows:

$$\boldsymbol{\epsilon}^{(e)}(\xi,\eta,t) = \begin{Bmatrix} \epsilon_x^{(e)}(\xi,\eta,t) \\ \epsilon_y^{(e)}(\xi,\eta,t) \\ \gamma_{xy}^{(e)}(\xi,\eta,t) \end{Bmatrix} = \begin{bmatrix} \mathbf{B}_x^{(e)}(\xi,\eta) \\ \mathbf{B}_y^{(e)}(\xi,\eta) \\ \mathbf{B}_{xy}^{(e)}(\xi,\eta) \end{bmatrix}\mathbf{q}^{(e)}(t) = \mathbf{B}^{(e)}(\xi,\eta)\mathbf{q}^{(e)}(t). \tag{23}$$

Next, having a way to evaluate strains inside the finite element domain, one aims to establish how stresses can be interpolated as functions of the element nodal DOFs. For an isotropic material, one can recourse to Hooke's law, which has been given in Eq. (7) for three-dimensional problems. Since two-dimensional elasticity is being considered, Hooke's law can be simplified, in order to address the two available possibilities:

(i) Plane stress In this case, $\sigma_z^{(e)} = \tau_{xz}^{(e)} = \tau_{yz}^{(e)} \equiv 0$. The remaining stresses can be evaluated using:

$$\begin{aligned}\boldsymbol{\sigma}^{(e)}(\xi,\eta,t) = \begin{Bmatrix} \sigma_x^{(e)}(\xi,\eta,t) \\ \sigma_y^{(e)}(\xi,\eta,t) \\ \tau_{xy}^{(e)}(\xi,\eta,t) \end{Bmatrix} &= \frac{E}{1-\nu^2}\begin{bmatrix} 1 & \nu & 0 \\ \nu & 1 & 0 \\ 0 & 0 & \frac{1-\nu}{2} \end{bmatrix}\begin{Bmatrix} \epsilon_x^{(e)}(\xi,\eta,t) \\ \epsilon_y^{(e)}(\xi,\eta,t) \\ \gamma_{xy}^{(e)}(\xi,\eta,t) \end{Bmatrix} \\ &= \mathbf{D}^{(e)}\boldsymbol{\epsilon}^{(e)}(\xi,\eta,t) = \mathbf{D}^{(e)}\mathbf{B}^{(e)}(\xi,\eta)\mathbf{q}^{(e)}(t). \end{aligned} \tag{24a}$$

Matrix $\mathbf{D}^{(e)}$ can be directly identified in the previous equation. While there is no stress on the plane whose normal is directed along z, a normal strain arises, due to the Poisson effect:

$$\epsilon_z^{(e)}(\xi,\eta,t) = -\frac{\nu}{E}\left[\sigma_x^{(e)}(\xi,\eta,t) + \sigma_y^{(e)}(\xi,\eta,t)\right]. \tag{24b}$$

The geometry of the solid is such that one of its characteristic dimensions (along z) is much smaller than the others, i.e. the solid is essentially a sheet, flat and thin. Applied loads are assumed to be distributed uniformly along the thickness.

(ii) Plane strain In this case, $\epsilon_z^{(e)} = \gamma_{xz}^{(e)} = \gamma_{yz}^{(e)} \equiv 0$. The stresses can be obtained from:

$$\begin{aligned}\boldsymbol{\sigma}^{(e)}(\xi,\eta,t) = \begin{Bmatrix}\sigma_x^{(e)}(\xi,\eta,t)\\ \sigma_y^{(e)}(\xi,\eta,t)\\ \tau_{xy}^{(e)}(\xi,\eta,t)\end{Bmatrix} &= \tfrac{E}{(1+\nu)(1-2\nu)}\begin{bmatrix}1-\nu & \nu & 0\\ \nu & 1-\nu & 0\\ 0 & 0 & \frac{1-2\nu}{2}\end{bmatrix}\begin{Bmatrix}\epsilon_x^{(e)}(\xi,\eta,t)\\ \epsilon_y^{(e)}(\xi,\eta,t)\\ \gamma_{xy}^{(e)}(\xi,\eta,t)\end{Bmatrix}\\ &= \mathbf{D}^{(e)}\boldsymbol{\epsilon}^{(e)}(\xi,\eta,t) = \mathbf{D}^{(e)}\mathbf{B}^{(e)}(\xi,\eta)\mathbf{q}^{(e)}(t),\end{aligned} \tag{25a}$$

and:

$$\sigma_z^{(e)}(\xi,\eta,t) = \frac{\nu E}{(1+\nu)(1-2\nu)}\left[\epsilon_x^{(e)}(\xi,\eta,t) + \epsilon_y^{(e)}(\xi,\eta,t)\right]. \tag{25b}$$

Matrix $\mathbf{D}^{(e)}$ can once again be determined for this case by inspecting the relations just presented. The case of plane strain is associated to solids which have one characteristic dimension (along z) much larger than the others, i.e. they correspond to right prisms. Applied loads are assumed to be distributed uniformly along the length (z-dimension) of the solid.

As can be seen, irrespective of the considered case, the relevant stresses can be obtained using a relationship of the type $\boldsymbol{\sigma}^{(e)}(\xi,\eta,t) = \mathbf{D}^{(e)}\boldsymbol{\epsilon}^{(e)}(\xi,\eta,t)$, with the constitutive matrix $\mathbf{D}^{(e)}$ taking distinct forms to accommodate for the possible scenarios.

We can now plug developed expressions in Eqs. (4) and (5) to evaluate the kinetic and potential energies related to the finite element under consideration. With regards to the first, we have:

$$\begin{aligned}\mathcal{K}^{(e)} &= \iiint_{\Omega_t^{(e)}} \frac{1}{2}\rho^{(e)}(x,y,z)\left\{\left[\dot{u}^{(e)}(x,y,z,t)\right]^2 + \left[\dot{v}^{(e)}(x,y,z,t)\right]^2\right\}\mathrm{d}x\,\mathrm{d}y\,\mathrm{d}z\\ &= \int_0^{L_z}\mathrm{d}z\int_{-1}^{1}\int_{-1}^{1}\frac{1}{2}\rho^{(e)}(\xi,\eta)\left\{\left[\dot{u}^{(e)}(\xi,\eta,t)\right]^2 + \left[\dot{v}^{(e)}(\xi,\eta,t)\right]^2\right\}\det\mathbf{J}^{(e)}\,\mathrm{d}\xi\,\mathrm{d}\eta\\ &= L_z\int_{-1}^{1}\int_{-1}^{1}\frac{1}{2}\rho^{(e)}\left[\dot{\mathbf{q}}^{(e)\mathrm{T}}\mathbf{N}_u^{(e)\mathrm{T}}\mathbf{N}_u^{(e)}\dot{\mathbf{q}}^{(e)} + \dot{\mathbf{q}}^{(e)\mathrm{T}}\mathbf{N}_v^{(e)\mathrm{T}}\mathbf{N}_v^{(e)}\dot{\mathbf{q}}^{(e)}\right]\det\mathbf{J}^{(e)}\,\mathrm{d}\xi\,\mathrm{d}\eta\\ &= \frac{1}{2}\dot{\mathbf{q}}^{(e)\mathrm{T}}(t)\left\{L_z\int_{-1}^{1}\int_{-1}^{1}\rho^{(e)}\left[\mathbf{N}_u^{(e)\mathrm{T}}\mathbf{N}_u^{(e)} + \mathbf{N}_v^{(e)\mathrm{T}}\mathbf{N}_v^{(e)}\right]\det\mathbf{J}^{(e)}\,\mathrm{d}\xi\,\mathrm{d}\eta\right\}\dot{\mathbf{q}}^{(e)}(t)\\ &= \frac{1}{2}\dot{\mathbf{q}}^{(e)\mathrm{T}}(t)\mathbf{M}^{(e)}\dot{\mathbf{q}}^{(e)}(t),\end{aligned} \tag{26}$$

where we note, for instance, that $\dot{u}^{(e)} = \mathbf{N}_u^{(e)}\dot{\mathbf{q}}^{(e)} = \dot{\mathbf{q}}^{(e)\mathrm{T}}\mathbf{N}_u^{(e)\mathrm{T}}$, since $\dot{u}^{(e)}$ is a scalar quantity; and this implies that $\left(\dot{u}^{(e)}\right)^2$ can be evaluate through $\dot{\mathbf{q}}^{(e)\mathrm{T}}\mathbf{N}_u^{(e)\mathrm{T}}\mathbf{N}_u^{(e)}\dot{\mathbf{q}}^{(e)}$. Similar remarks hold for the other terms which contribute to the kinetic energy expression. One also should point out that L_z corresponds to the thickness of the finite element. From the last two lines of the previous equation,

$$\mathbf{M}^{(e)} = L_z\int_{-1}^{1}\int_{-1}^{1}\rho^{(e)}\left[\mathbf{N}_u^{(e)\mathrm{T}}\mathbf{N}_u^{(e)} + \mathbf{N}_v^{(e)\mathrm{T}}\mathbf{N}_v^{(e)}\right]\det\mathbf{J}^{(e)}\,\mathrm{d}\xi\,\mathrm{d}\eta, \tag{27}$$

which is recognized as the finite element mass matrix. It is symmetric, positive definite, and can be evaluated analytically, with the aid of symbolic algebra software; or using numerical integration techniques, such as Gauss-Legendre quadrature (as is done in codes which are made available with this material). This latter option is interesting because the integration of polynomials can be performed exactly, while demanding a low computational cost. While not directly related to the formulation which is being considered here, numerical integration of finite element matrices or load vectors can also be resorted to: (i) for avoiding issues related to locking-phenomena (which depends on the finite element formulation), by performing reduced integration of relevant quantities; and/or (ii) for enabling nonlinear analyzes, in which system matrices and/or load vectors change with respect to the system configuration [Bathe, 2014, de Borst et al., 2012].

With regards to the potential energy contribution due to externally applied forces, we have:

$$
\begin{aligned}
\mathcal{W}_{\text{ext}}^{(e)} &= \iiint_{\Omega_t^{(e)}} \begin{bmatrix} u^{(e)}(x,y,t) & v^{(e)}(x,y,t) \end{bmatrix} \begin{Bmatrix} f_b^x(x,y,t) \\ f_b^y(x,y,t) \end{Bmatrix} \mathrm{d}x\,\mathrm{d}y\,\mathrm{d}z \\
&\quad + \iint_{\partial\Omega_t^{(e)}} \begin{bmatrix} u^{(e)}(x,y,t) & v^{(e)}(x,y,t) \end{bmatrix} \begin{Bmatrix} f_s^x(x,y,t) \\ f_s^y(x,y,t) \end{Bmatrix} \mathrm{d}S \\
&= L_z \int_{-1}^{1}\int_{-1}^{1} \begin{bmatrix} u^{(e)}(\xi,\eta,t) & v^{(e)}(\xi,\eta,t) \end{bmatrix} \begin{Bmatrix} f_b^x(\xi,\eta,t) \\ f_b^y(\xi,\eta,t) \end{Bmatrix} \det \mathbf{J}^{(e)}\, \mathrm{d}\xi\,\mathrm{d}\eta \\
&\quad + L_z \int_{-1}^{1} \begin{bmatrix} u^{(e)}(-1,\eta,t) & v^{(e)}(-1,\eta,t) \end{bmatrix} \begin{Bmatrix} f_s^x(-1,\eta,t) \\ f_s^y(-1,\eta,t) \end{Bmatrix} \left.\sqrt{\left(\frac{\partial x}{\partial \eta}\right)^2 + \left(\frac{\partial y}{\partial \eta}\right)^2}\,\right|_{\xi=-1} \mathrm{d}\eta \\
&\quad + L_z \int_{-1}^{1} \begin{bmatrix} u^{(e)}(1,\eta,t) & v^{(e)}(1,\eta,t) \end{bmatrix} \begin{Bmatrix} f_s^x(1,\eta,t) \\ f_s^y(1,\eta,t) \end{Bmatrix} \left.\sqrt{\left(\frac{\partial x}{\partial \eta}\right)^2 + \left(\frac{\partial y}{\partial \eta}\right)^2}\,\right|_{\xi=1} \mathrm{d}\eta \\
&\quad + L_z \int_{-1}^{1} \begin{bmatrix} u^{(e)}(\xi,-1,t) & v^{(e)}(\xi,-1,t) \end{bmatrix} \begin{Bmatrix} f_s^x(\xi,-1,t) \\ f_s^y(\xi,-1,t) \end{Bmatrix} \left.\sqrt{\left(\frac{\partial x}{\partial \xi}\right)^2 + \left(\frac{\partial y}{\partial \xi}\right)^2}\,\right|_{\eta=-1} \mathrm{d}\xi \\
&\quad + L_z \int_{-1}^{1} \begin{bmatrix} u^{(e)}(\xi,1,t) & v^{(e)}(\xi,1,t) \end{bmatrix} \begin{Bmatrix} f_s^x(\xi,1,t) \\ f_s^y(\xi,1,t) \end{Bmatrix} \left.\sqrt{\left(\frac{\partial x}{\partial \xi}\right)^2 + \left(\frac{\partial y}{\partial \xi}\right)^2}\,\right|_{\eta=1} \mathrm{d}\xi \\
&= \mathbf{q}^{(e)^{\mathrm{T}}} \left\{ L_z \int_{-1}^{1}\int_{-1}^{1} \begin{bmatrix} \mathbf{N}_u^{(e)^{\mathrm{T}}}(\xi,\eta) & \mathbf{N}_v^{(e)^{\mathrm{T}}}(\xi,\eta) \end{bmatrix} \begin{Bmatrix} f_b^x(\xi,\eta,t) \\ f_b^y(\xi,\eta,t) \end{Bmatrix} \det \mathbf{J}^{(e)}\, \mathrm{d}\xi\,\mathrm{d}\eta \right\} \\
&+ \mathbf{q}^{(e)^{\mathrm{T}}} \left\{ L_z \int_{-1}^{1} \begin{bmatrix} \mathbf{N}_u^{(e)^{\mathrm{T}}}(-1,\eta) & \mathbf{N}_v^{(e)^{\mathrm{T}}}(-1,\eta) \end{bmatrix} \begin{Bmatrix} f_s^x(-1,\eta,t) \\ f_s^y(-1,\eta,t) \end{Bmatrix} \left.\sqrt{\left(\frac{\partial x}{\partial \eta}\right)^2 + \left(\frac{\partial y}{\partial \eta}\right)^2}\,\right|_{\xi=-1} \mathrm{d}\eta \right. \\
&\qquad + L_z \int_{-1}^{1} \begin{bmatrix} \mathbf{N}_u^{(e)^{\mathrm{T}}}(1,\eta) & \mathbf{N}_v^{(e)^{\mathrm{T}}}(1,\eta) \end{bmatrix} \begin{Bmatrix} f_s^x(1,\eta,t) \\ f_s^y(1,\eta,t) \end{Bmatrix} \left.\sqrt{\left(\frac{\partial x}{\partial \eta}\right)^2 + \left(\frac{\partial y}{\partial \eta}\right)^2}\,\right|_{\xi=1} \mathrm{d}\eta \\
&\qquad + L_z \int_{-1}^{1} \begin{bmatrix} \mathbf{N}_u^{(e)^{\mathrm{T}}}(\xi,-1) & \mathbf{N}_v^{(e)^{\mathrm{T}}}(\xi,-1) \end{bmatrix} \begin{Bmatrix} f_s^x(\xi,-1,t) \\ f_s^y(\xi,-1,t) \end{Bmatrix} \left.\sqrt{\left(\frac{\partial x}{\partial \xi}\right)^2 + \left(\frac{\partial y}{\partial \xi}\right)^2}\,\right|_{\eta=-1} \mathrm{d}\xi \\
&\qquad \left. + L_z \int_{-1}^{1} \begin{bmatrix} \mathbf{N}_u^{(e)^{\mathrm{T}}}(\xi,1) & \mathbf{N}_v^{(e)^{\mathrm{T}}}(\xi,1) \end{bmatrix} \begin{Bmatrix} f_s^x(\xi,1,t) \\ f_s^y(\xi,1,t) \end{Bmatrix} \left.\sqrt{\left(\frac{\partial x}{\partial \xi}\right)^2 + \left(\frac{\partial y}{\partial \xi}\right)^2}\,\right|_{\eta=1} \mathrm{d}\xi \right\} \\
&= \mathbf{q}^{(e)^{\mathrm{T}}}(t)\mathbf{Q}_b^{(e)}(t) + \mathbf{q}^{(e)^{\mathrm{T}}}(t)\mathbf{Q}_s^{(e)}(t),
\end{aligned} \tag{28}
$$

where we considered $\mathrm{d}S = \mathrm{d}z\,\mathrm{d}l$, with $\mathrm{d}l$ corresponding to a differential length on the boundary of the finite element. The sides of the element (which in our case are straight lines) can be described by the parametrizations $(x(\eta), y(\eta))$ for $\xi = \pm 1$ or $(x(\xi), y(\xi))$ for $\eta = \pm 1$, such that $\mathrm{d}l = \sqrt{\left(\frac{\partial x}{\partial \eta}\right)^2 + \left(\frac{\partial y}{\partial \eta}\right)^2}\mathrm{d}\eta$ or $\mathrm{d}l = \sqrt{\left(\frac{\partial x}{\partial \xi}\right)^2 + \left(\frac{\partial y}{\partial \xi}\right)^2}\mathrm{d}\xi$, respectively. The square-root terms in the previous expressions for $\mathrm{d}l$ are necessary to take into account the parametrization adopted for the boundary curves. It is also worth noticing that, for evaluating the load vector $\mathbf{Q}_s^{(e)}(t)$, the finite element boundary is split — contributions due to the each side of the finite element are treated separately, for convenience.

In order to evaluate both $\mathbf{Q}_b^{(e)}(t)$ and $\mathbf{Q}_s^{(e)}(t)$, it is useful to consider that:

$$\mathbf{f}_b^{(e)} = \begin{Bmatrix} f_b^x(\xi,\eta,t) \\ f_b^y(\xi,\eta,t) \end{Bmatrix} = \begin{Bmatrix} \bar{f}_b^x(\xi,\eta) g_b^x(t) \\ \bar{f}_b^y(\xi,\eta) g_b^y(t) \end{Bmatrix} = \begin{bmatrix} \bar{f}_b^x(\xi,\eta) & 0 \\ 0 & \bar{f}_b^y(\xi,\eta) \end{bmatrix} \begin{Bmatrix} g_b^x(t) \\ g_b^y(t) \end{Bmatrix} = \bar{\mathbf{f}}_b^{(e)}(\xi,\eta)\mathbf{g}_b^{(e)}(t); \tag{29a}$$

$$\mathbf{f}_s^{(e)} = \begin{Bmatrix} f_s^x(\xi,\eta,t) \\ f_s^y(\xi,\eta,t) \end{Bmatrix} = \begin{Bmatrix} \bar{f}_s^x(\xi,\eta) g_s^x(t) \\ \bar{f}_s^y(\xi,\eta) g_s^y(t) \end{Bmatrix} = \begin{bmatrix} \bar{f}_s^x(\xi,\eta) & 0 \\ 0 & \bar{f}_s^y(\xi,\eta) \end{bmatrix} \begin{Bmatrix} g_s^x(t) \\ g_s^y(t) \end{Bmatrix} = \bar{\mathbf{f}}_s^{(e)}(\xi,\eta)\mathbf{g}_s^{(e)}(t). \tag{29b}$$

Furthermore, we assume that the surface loads can vary linearly between the finite element's nodes:

$$\begin{Bmatrix} \bar{f}_s^x(\xi,-1) \\ \bar{f}_s^y(\xi,-1) \end{Bmatrix} = \begin{Bmatrix} p_{12,1}^x \\ p_{12,1}^y \end{Bmatrix} \frac{1}{2}(1-\xi) + \begin{Bmatrix} p_{12,2}^x \\ p_{12,2}^y \end{Bmatrix} \frac{1}{2}(1+\xi); \tag{30a}$$

$$\begin{Bmatrix} \bar{f}_s^x(1,\eta) \\ \bar{f}_s^y(1,\eta) \end{Bmatrix} = \begin{Bmatrix} p_{23,2}^x \\ p_{23,2}^y \end{Bmatrix} \frac{1}{2}(1-\eta) + \begin{Bmatrix} p_{23,3}^x \\ p_{23,3}^y \end{Bmatrix} \frac{1}{2}(1+\eta); \tag{30b}$$

$$\begin{Bmatrix} \bar{f}_s^x(\xi,1) \\ \bar{f}_s^y(\xi,1) \end{Bmatrix} = \begin{Bmatrix} p_{34,3}^x \\ p_{34,3}^y \end{Bmatrix} \frac{1}{2}(1+\xi) + \begin{Bmatrix} p_{34,4}^x \\ p_{34,4}^y \end{Bmatrix} \frac{1}{2}(1-\xi); \tag{30c}$$

$$\begin{Bmatrix} \bar{f}_s^x(-1,\eta) \\ \bar{f}_s^y(-1,\eta) \end{Bmatrix} = \begin{Bmatrix} p_{41,4}^x \\ p_{41,4}^y \end{Bmatrix} \frac{1}{2}(1+\eta) + \begin{Bmatrix} p_{41,1}^x \\ p_{41,1}^y \end{Bmatrix} \frac{1}{2}(1-\eta), \tag{30d}$$

in which $p_{ij,i}^x$, $p_{ij,i}^y$ represent loads per unit area applied on node i along the finite element side between nodes i and j.

Based on the previous developments, we can see that:

$$\mathbf{Q}_b^{(e)}(t) = L_z \left\{ \int_{-1}^{1} \int_{-1}^{1} \begin{bmatrix} \mathbf{N}_u^{(e)\mathrm{T}}(\xi,\eta) & \mathbf{N}_v^{(e)\mathrm{T}}(\xi,\eta) \end{bmatrix} \bar{\mathbf{f}}_b^{(e)}(\xi,\eta) \det \mathbf{J}^{(e)} \, \mathrm{d}\xi \, \mathrm{d}\eta \right\} \mathbf{g}_b^{(e)}(t); \tag{31}$$

$$\begin{aligned} \mathbf{Q}_s^{(e)}(t) = L_z \Bigg\{ & \sum_{\bar{\xi} \in \{-1,1\}} \int_{-1}^{1} \begin{bmatrix} \mathbf{N}_u^{(e)\mathrm{T}}(\bar{\xi},\eta) & \mathbf{N}_v^{(e)\mathrm{T}}(\bar{\xi},\eta) \end{bmatrix} \bar{\mathbf{f}}_s^{(e)}(\bar{\xi},\eta) \left. \sqrt{\left(\frac{\partial x}{\partial \eta}\right)^2 + \left(\frac{\partial y}{\partial \eta}\right)^2} \right|_{\xi=\bar{\xi}} \mathrm{d}\eta \\ & + \sum_{\bar{\eta} \in \{-1,1\}} \int_{-1}^{1} \begin{bmatrix} \mathbf{N}_u^{(e)\mathrm{T}}(\xi,\bar{\eta}) & \mathbf{N}_v^{(e)\mathrm{T}}(\xi,\bar{\eta}) \end{bmatrix} \bar{\mathbf{f}}_s^{(e)}(\xi,\bar{\eta}) \left. \sqrt{\left(\frac{\partial x}{\partial \xi}\right)^2 + \left(\frac{\partial y}{\partial \xi}\right)^2} \right|_{\eta=\bar{\eta}} \mathrm{d}\xi \Bigg\} \mathbf{g}_s^{(e)}(t). \end{aligned} \tag{32}$$

Having established Eq. (28), we consider Eq. (5) in order to obtain:

$$\begin{aligned}
\mathcal{U}^{(e)} &= \frac{1}{2}\iiint_{\Omega_t^{(e)}} \left[\sigma_x^{(e)}\epsilon_x^{(e)} + \sigma_y^{(e)}\epsilon_y^{(e)} + \tau_{xy}^{(e)}\gamma_{xy}^{(e)}\right] \mathrm{d}x\,\mathrm{d}y\,\mathrm{d}z - \mathcal{W}_{\text{ext}} \\
&= \frac{1}{2}L_z \int_{-1}^{1}\int_{-1}^{1} \boldsymbol{\sigma}^{(e)^{\mathrm{T}}}(\xi,\eta,t)\boldsymbol{\epsilon}^{(e)}(\xi,\eta,t)\det\mathbf{J}^{(e)}\,\mathrm{d}\xi\,\mathrm{d}\eta - \mathbf{q}^{(e)^{\mathrm{T}}}\left[\mathbf{Q}_b^{(e)}(t) + \mathbf{Q}_s^{(e)}(t)\right] \\
&= \frac{1}{2}\mathbf{q}^{(e)^{\mathrm{T}}}\left\{L_z \int_{-1}^{1}\int_{-1}^{1} \mathbf{B}^{(e)^{\mathrm{T}}}\mathbf{D}^{(e)}\mathbf{B}^{(e)}\det\mathbf{J}^{(e)}\,\mathrm{d}\xi\,\mathrm{d}\eta\right\}\mathbf{q}^{(e)}(t) - \mathbf{q}^{(e)^{\mathrm{T}}}\left[\mathbf{Q}_b^{(e)}(t) + \mathbf{Q}_s^{(e)}(t)\right] \\
&= \frac{1}{2}\mathbf{q}^{(e)^{\mathrm{T}}}(t)\mathbf{K}^{(e)}\mathbf{q}^{(e)}(t) - \mathbf{q}^{(e)^{\mathrm{T}}}(t)\left[\mathbf{Q}_b^{(e)}(t) + \mathbf{Q}_s^{(e)}(t)\right],
\end{aligned} \tag{33}$$

where Eqs. (24a), (25a) were used, together with the fact that $\mathbf{D}^{(e)}$ is a symmetric matrix. We see that:

$$\mathbf{K}^{(e)} = L_z \int_{-1}^{1}\int_{-1}^{1} \mathbf{B}^{(e)^{\mathrm{T}}}\mathbf{D}^{(e)}\mathbf{B}^{(e)}\det\mathbf{J}^{(e)}\,\mathrm{d}\xi\,\mathrm{d}\eta, \tag{34}$$

which is known as the finite element stiffness matrix – which is symmetric, and positive semi-definite.

By considering the earlier developments, the Lagrangian becomes:

$$\mathcal{L}^{(e)} = \frac{1}{2}\dot{\mathbf{q}}^{(e)^{\mathrm{T}}}(t)\mathbf{M}^{(e)}\dot{\mathbf{q}}^{(e)}(t) - \left\{\frac{1}{2}\mathbf{q}^{(e)^{\mathrm{T}}}(t)\mathbf{K}^{(e)}\mathbf{q}^{(e)}(t) - \mathbf{q}^{(e)^{\mathrm{T}}}(t)\left[\mathbf{Q}_b^{(e)}(t) + \mathbf{Q}_s^{(e)}(t)\right]\right\}. \tag{35}$$

Now, according to the Variational Principles of Mechanics, to make the relevant action functional stationary, the Lagrangian must be such that it complies with the Euler-Lagrange equations [Lanczos, 1986]:

$$\frac{\mathrm{d}}{\mathrm{d}t}\left(\frac{\partial\mathcal{L}^{(e)}}{\partial\dot{\mathbf{q}}^{(e)}}\right) - \frac{\partial\mathcal{L}^{(e)}}{\partial\mathbf{q}^{(e)}} = \mathbf{Q}_{\text{nc}}^{(e)}, \tag{36}$$

where $\mathbf{Q}_{\text{nc}}^{(e)}$ collects the non-conservative generalized loads. (These can be obtained by calculating the virtual work of the non-conservative actions.) The derivatives of the scalar function $\mathcal{L}^{(e)}$ with respect to the vectors $\mathbf{q}^{(e)}$ and $\dot{\mathbf{q}}^{(e)}$ produce vectors, whose components are given by the derivative of $\mathcal{L}^{(e)}$ with respect to the components of $\mathbf{q}^{(e)}$ and $\dot{\mathbf{q}}^{(e)}$, respectively. By substituting the Lagrangian expression given in Eq. (35), we are finally able to obtain the equations of motion for the finite element:

$$\mathbf{M}^{(e)}\ddot{\mathbf{q}}^{(e)}(t) + \mathbf{K}^{(e)}\mathbf{q}^{(e)}(t) = \mathbf{Q}_{\text{nc}}^{(e)}(t) + \mathbf{Q}_b^{(e)}(t) + \mathbf{Q}_s^{(e)}(t), \tag{37}$$

which correspond to the input-output relationship one has sought during this subsection. This set of coupled, second-order, linear ordinary differential equations relate the nodal DOFs to loads that are ultimately applied at the element nodes. For instance, conservative distributed loads have been replaced by equivalent nodal contributions when one has put forward Eqs. (31) and (32).

2.1.3 Formulation at global level

The previous developments have addressed the mathematical formulation related to a single finite element of the considered type. In a practical application, various elements are combined in a mesh, to better represent the geometry of the continuum body or structure; and also to enable a good approximation of the exact response for the underlying model equations (being them differential or algebraic, cf. our discussion along section 1). In this sense, we have to remind ourselves that interpolation functions have been proposed to represent the field variables inside the element domain. Typically, the adopted interpolation schemes are not adequate to represent the response of the structure or continuum body over its entire domain, i.e. the interpolation functions which are used are able to approximate responses only locally.

To assemble a finite element mesh, two basic conditions need to be fulfilled at every node of the mesh: (i) compatibility of field variables; and (ii) in the case of structural analyses, dynamic equilibrium of loads. It is important to realize that these conditions are fulfilled only at the nodes of the mesh. Hence, there is not guarantee that dynamic equilibrium is assured across boundaries of finite elements (unless at shared nodes).

For the purpose of abiding by these requirements, we initially attribute the required DOFs to each node of the complete finite element mesh, to make a global list of DOFs, which are collected in a vector $\mathbf{q}^{(g)}$. From this list, for a particular finite element e of the mesh, we can identify the relevant DOFs, which are those related to its nodes. Mathematically, this can be accomplished by constructing a Boolean "localization" matrix $\mathbf{L}^{(e)}$, such that:

$$\mathbf{q}^{(e)} = \mathbf{L}^{(e)}\mathbf{q}^{(g)}. \tag{38}$$

If our finite element mesh has $n^{(g)}$ DOFs, and each element of the mesh has four nodes with two DOFs per node, then $\mathbf{L}^{(e)}$ has size $8 \times n^{(g)}$.

For each finite element of the mesh, we can write Eq. (35). To obtain the Lagrangian of the complete structure, we can simply sum the contributions of all finite elements of the mesh:

$$\begin{aligned}
\mathcal{L}^{(g)} = \sum_{e=1}^{n_{\text{ele}}} \mathcal{L}^{(e)} &= \sum_{e=1}^{n_{\text{ele}}} \frac{1}{2}\dot{\mathbf{q}}^{(e)^{\mathrm{T}}}(t)\mathbf{M}^{(e)}\dot{\mathbf{q}}^{(e)}(t) - \sum_{e=1}^{n_{\text{ele}}} \frac{1}{2}\mathbf{q}^{(e)^{\mathrm{T}}}(t)\mathbf{K}^{(e)}\mathbf{q}^{(e)}(t) \\
&\qquad + \sum_{e=1}^{n_{\text{ele}}} \mathbf{q}^{(e)^{\mathrm{T}}}(t)\left[\mathbf{Q}_b^{(e)}(t) + \mathbf{Q}_s^{(e)}(t)\right] \\
&= \sum_{e=1}^{n_{\text{ele}}} \frac{1}{2}\dot{\mathbf{q}}^{(g)^{\mathrm{T}}}(t)\mathbf{L}^{(e)^{\mathrm{T}}}\mathbf{M}^{(e)}\mathbf{L}^{(e)}\dot{\mathbf{q}}^{(g)}(t) - \sum_{e=1}^{n_{\text{ele}}} \frac{1}{2}\mathbf{q}^{(g)^{\mathrm{T}}}(t)\mathbf{L}^{(e)^{\mathrm{T}}}\mathbf{K}^{(e)}\mathbf{L}^{(e)}\mathbf{q}^{(g)}(t) \\
&\qquad + \sum_{e=1}^{n_{\text{ele}}} \mathbf{q}^{(g)^{\mathrm{T}}}(t)\left[\mathbf{L}^{(e)^{\mathrm{T}}}\mathbf{Q}_b^{(e)}(t) + \mathbf{L}^{(e)^{\mathrm{T}}}\mathbf{Q}_s^{(e)}(t)\right] \\
&= \frac{1}{2}\dot{\mathbf{q}}^{(g)^{\mathrm{T}}}(t)\left[\sum_{e=1}^{n_{\text{ele}}} \mathbf{L}^{(e)^{\mathrm{T}}}\mathbf{M}^{(e)}\mathbf{L}^{(e)}\right]\dot{\mathbf{q}}^{(g)}(t) - \frac{1}{2}\mathbf{q}^{(g)^{\mathrm{T}}}(t)\left[\sum_{e=1}^{n_{\text{ele}}} \mathbf{L}^{(e)^{\mathrm{T}}}\mathbf{K}^{(e)}\mathbf{L}^{(e)}\right]\mathbf{q}^{(g)}(t) \\
&\qquad + \mathbf{q}^{(g)^{\mathrm{T}}}(t)\sum_{e=1}^{n_{\text{ele}}}\left[\mathbf{L}^{(e)^{\mathrm{T}}}\mathbf{Q}_b^{(e)}(t) + \mathbf{L}^{(e)^{\mathrm{T}}}\mathbf{Q}_s^{(e)}(t)\right] \\
&= \frac{1}{2}\dot{\mathbf{q}}^{(g)^{\mathrm{T}}}(t)\mathbf{M}^{(g)}\dot{\mathbf{q}}^{(g)}(t) - \frac{1}{2}\mathbf{q}^{(g)^{\mathrm{T}}}(t)\mathbf{K}^{(g)}\mathbf{q}^{(g)}(t) + \mathbf{q}^{(g)^{\mathrm{T}}}(t)\left[\mathbf{Q}_b^{(g)}(t) + \mathbf{Q}_s^{(g)}(t)\right],
\end{aligned} \tag{39}$$

in which:

$$\mathbf{M}^{(g)} = \sum_{e=1}^{n_{\text{ele}}} \mathbf{L}^{(e)^{\mathrm{T}}}\mathbf{M}^{(e)}\mathbf{L}^{(e)} \qquad \text{and} \qquad \mathbf{K}^{(g)} = \sum_{e=1}^{n_{\text{ele}}} \mathbf{L}^{(e)^{\mathrm{T}}}\mathbf{K}^{(e)}\mathbf{L}^{(e)} \tag{40}$$

are the global mass and stiffness matrices, respectively. For the considered case, these are symmetric. Also, due to how the global matrices are assembled, they are frequently sparse and banded, specially when the complete finite element model possess a large number of nodes/DOFs. These facts can be exploited by solution algorithms to speed up computations and/or alleviate computer memory availability requirements. Regarding conservative body and surface loads, we see from the previous developments that their global form can be obtained from:

$$\mathbf{Q}_b^{(g)}(t) = \sum_{e=1}^{n_{\text{ele}}} \mathbf{L}^{(e)^{\mathrm{T}}}\mathbf{Q}_b^{(e)}(t) \qquad \text{and} \qquad \mathbf{Q}_s^{(g)}(t) = \sum_{e=1}^{n_{\text{ele}}} \mathbf{L}^{(e)^{\mathrm{T}}}\mathbf{Q}_s^{(e)}(t). \tag{41}$$

Having established Eq. (39), the Euler-Lagrange equations, applied to the global Lagrangian, then lead to the global equations of motion:

$$\mathbf{M}^{(g)}\ddot{\mathbf{q}}^{(g)}(t) + \mathbf{K}^{(g)}\mathbf{q}^{(g)}(t) = \mathbf{Q}_{\text{nc}}^{(g)}(t) + \mathbf{Q}_b^{(g)}(t) + \mathbf{Q}_s^{(g)}(t). \tag{42}$$

Since we are considering linear structural behavior, we have obtained a set of linear, second-order, ordinary differential equations to model the motion of a continuum solid body under plane-stress or plane-strain conditions. In essence, the finite element method was used to spatially discretize the partial differential equations (of infinite dimension in space and time) which apply under the same underlying assumptions. The resulting system of ordinary differential equations can be analyzed in various forms, as discussed in section 3 with examples.

2.2 Rectangular Kirchhoff-Love plate, equivalent single layer laminate finite element

2.2.1 Kinematics

To provide another example of the formulation of a finite element, we now address the case of a plate which is subjected to bending motion, whose kinematic behavior can be described by the Kirchhoff-Love plate theory. In this setting, some assumptions should hold: (i) straight lines normal to the mid-surface remain straight and normal to the mid-surface after deformation; and (ii) the thickness of the plate does not change during its motion. This theory is more adequate for plates of small thickness. Referring to Fig. 6, due to the previous hypotheses, and also taking into account that displacements are small (infinitesimal), we can see that the rotation and the displacement fields can be expressed according to:

$$w(x,y,z,t) = w_0(x,y,t); \qquad \theta_x(x,y,t) = \frac{\partial w_0(x,y,t)}{\partial y}; \qquad \theta_y(x,y,t) = -\frac{\partial w_0(x,y,t)}{\partial x};$$
$$u(x,y,z,t) = u_0(x,y,t) + z\theta_y(x,y,t); \qquad v(x,y,z,t) = v_0(x,y,t) - z\theta_x(x,y,t), \quad (43)$$

where the transversal displacement w is assumed to be independent of z.

The strains can then be evaluated with the help of Eq. (8) as:

$$\epsilon_x = \frac{\partial u_0(x,y,t)}{\partial x} - z\frac{\partial^2 w_0(x,y,t)}{\partial x^2}, \qquad \epsilon_y = \frac{\partial v_0(x,y,t)}{\partial y} - z\frac{\partial^2 w_0(x,y,t)}{\partial y^2},$$
$$\gamma_{xy} = \frac{\partial u_0(x,y,t)}{\partial y} + \frac{\partial v_0(x,y,t)}{\partial x} - 2z\frac{\partial^2 w_0(x,y,t)}{\partial x \partial y}, \qquad \epsilon_z = \gamma_{xz} = \gamma_{xz} \equiv 0. \quad (44)$$

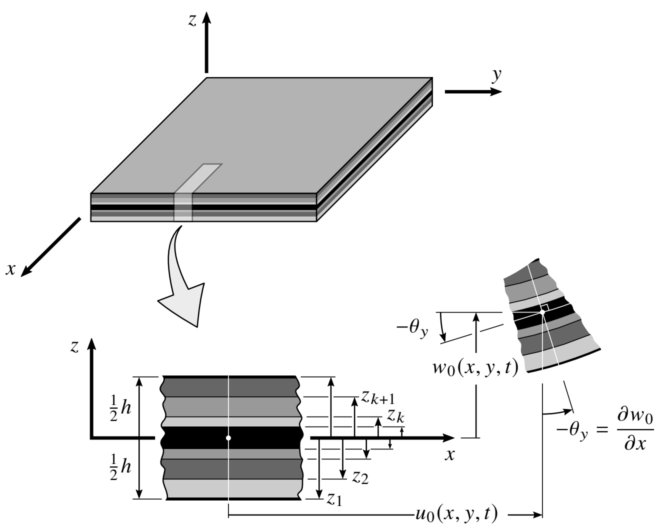

Figure 6: Plate (laminate) kinematic behavior along x-z plane according to Kirchhoff-Love theory.

2.2.2 Element geometry and interpolation of field variables

The finite element we consider here to model plate bending is but one of several which are available for this problem. If more detailed literature is consulted, the reader should see that conforming and non-conforming plate elements exist [Bathe, 2014, Reddy, 2019]. The one presented by us here is of the latter type, which means it does not guarantee continuity of the normal slope across the boundaries of finite elements which are neighbors. This issue results due to the formulation of the finite element itself (i.e. it is related to the interpolation functions which are adopted and the number of nodes of the element). Being it a non-conforming finite element, convergence of results can become problematic, especially if coarse meshes are employed.

Fig. 7 shows the geometry of the plate element. It is rectangular (not an arbitrary quadrilateral), with only four nodes. The nodal DOFs directly related to bending are $w_{0,i}^{(e)}(t) = w_0^{(e)}(x_i, y_i, t)$, $\theta_{x,i}^{(e)}(t) = \theta_x^{(e)}(x_i, y_i, t)$ and $\theta_{y,i}^{(e)}(t) = \theta_y^{(e)}(x_i, y_i, t)$, for $i \in \{1, 2, 3, 4\}$. The other DOFs, related to in-plane motions, are $u_{0,i}^{(e)}(t) = u_0^{(e)}(x_i, y_i, t)$ and $v_{0,i}^{(e)}(t) = v_0^{(e)}(x_i, y_i, t)$. Interpolation of the latter two can be performed according to Eqs. (13)–(15). For the remaining fields, we adopt [Junior et al., 2009]:

$$
\begin{aligned}
w_0^{(e)} = &\left[1 \quad x \quad y \quad x^2 \quad xy \quad y^2 \quad x^3 \quad x^2y \quad xy^2 \quad y^3 \quad x^3y \quad xy^3\right] \times \\
&\times \left\{a_{00} \quad a_{10} \quad a_{01} \quad a_{20} \quad a_{11} \quad a_{02} \quad a_{30} \quad a_{21} \quad a_{12} \quad a_{03} \quad a_{31} \quad a_{13}\right\}^{\mathrm{T}} = \mathbf{P}(x, y)\,\mathbf{a}(t);
\end{aligned} \tag{45a}
$$

$$
\begin{aligned}
\theta_x^{(e)} = \frac{\partial w_0^{(e)}(x, y, t)}{\partial x} = &\left[0 \quad 1 \quad 0 \quad 2x \quad y \quad 0 \quad 3x^2 \quad 2xy \quad y^2 \quad 0 \quad 3x^2y \quad y^3\right] \times \\
&\times \left\{a_{00} \quad a_{10} \quad a_{01} \quad a_{20} \quad a_{11} \quad a_{02} \quad a_{30} \quad a_{21} \quad a_{12} \quad a_{03} \quad a_{31} \quad a_{13}\right\}^{\mathrm{T}} = \frac{\partial \mathbf{P}}{\partial y}(x, y)\,\mathbf{a}(t);
\end{aligned} \tag{45b}
$$

$$
\begin{aligned}
\theta_y^{(e)} = \frac{\partial w_0^{(e)}(x, y, t)}{\partial y} = &\left[0 \quad 0 \quad 1 \quad 0 \quad x \quad 2y \quad 0 \quad x^2 \quad 2xy \quad 3y^2 \quad x^3 \quad 3xy^2\right] \times \\
&\times \left\{a_{00} \quad a_{10} \quad a_{01} \quad a_{20} \quad a_{11} \quad a_{02} \quad a_{30} \quad a_{21} \quad a_{12} \quad a_{03} \quad a_{31} \quad a_{13}\right\}^{\mathrm{T}} = -\frac{\partial \mathbf{P}}{\partial x}(x, y)\,\mathbf{a}(t),
\end{aligned} \tag{45c}
$$

where $\mathbf{P}$ is a row-matrix containing polynomials, and the column vector $\mathbf{a}$ comprises time-dependent

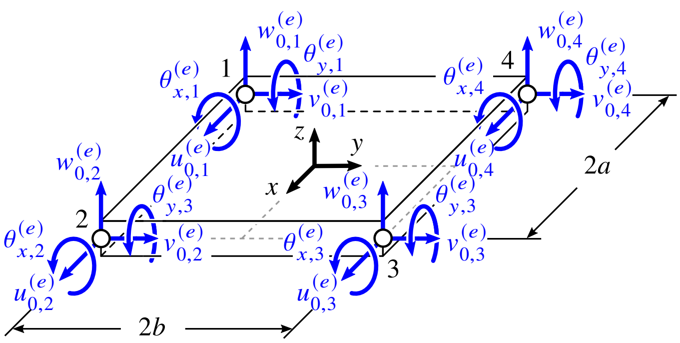

Figure 7: Non-conforming, rectangular plate (laminate) finite element with four nodes.

weights. The latter can be expressed in terms of the element nodal DOFs by enforcing:

$$\bar{\mathbf{q}}^{(e)}(t) = \begin{Bmatrix} w_{0,1}^{(e)}(t) \\ \theta_{x,1}^{(e)}(t) \\ \theta_{y,1}^{(e)}(t) \\ w_{0,2}^{(e)}(t) \\ \theta_{x,2}^{(e)}(t) \\ \theta_{y,2}^{(e)}(t) \\ w_{0,3}^{(e)}(t) \\ \theta_{x,3}^{(e)}(t) \\ \theta_{y,3}^{(e)}(t) \\ w_{0,4}^{(e)}(t) \\ \theta_{x,4}^{(e)}(t) \\ \theta_{y,4}^{(e)}(t) \end{Bmatrix} = \begin{bmatrix} \mathbf{P}(x_1, y_1) \\ \frac{\partial \mathbf{P}}{\partial y}(x_1, y_1) \\ -\frac{\partial \mathbf{P}}{\partial x}(x_1, y_1) \\ \mathbf{P}(x_2, y_2) \\ \frac{\partial \mathbf{P}}{\partial y}(x_2, y_2) \\ -\frac{\partial \mathbf{P}}{\partial x}(x_2, y_2) \\ \mathbf{P}(x_3, y_3) \\ \frac{\partial \mathbf{P}}{\partial y}(x_3, y_3) \\ -\frac{\partial \mathbf{P}}{\partial x}(x_3, y_3) \\ \mathbf{P}(x_4, y_4) \\ \frac{\partial \mathbf{P}}{\partial y}(x_4, y_4) \\ -\frac{\partial \mathbf{P}}{\partial x}(x_4, y_4) \end{bmatrix} \mathbf{a}(t) = \mathbf{A}\mathbf{a}(t) \qquad \Rightarrow \qquad \mathbf{a}(t) = \mathbf{A}^{-1}\bar{\mathbf{q}}^{(e)}(t). \tag{46}$$

Combining this last result with Eqs. (45), we are able to obtain the FE interpolation function matrices for the relevant displacement fields:

$$w_0^{(e)}(x, y, t) = \bar{\mathbf{N}}_w^{(e)}(x, y)\bar{\mathbf{q}}^{(e)}(t) = \left(\mathbf{P}(x, y)\mathbf{A}^{-1}\right)\bar{\mathbf{q}}^{(e)}(t); \tag{47a}$$

$$\theta_x^{(e)}(x, y, t) = \bar{\mathbf{N}}_{\theta_x}^{(e)}(x, y)\bar{\mathbf{q}}^{(e)}(t) = \left(\frac{\partial \mathbf{P}}{\partial y}(x, y)\mathbf{A}^{-1}\right)\bar{\mathbf{q}}^{(e)}(t); \tag{47b}$$

$$\theta_y^{(e)}(x, y, t) = \bar{\mathbf{N}}_{\theta_y}^{(e)}(x, y)\bar{\mathbf{q}}^{(e)}(t) = \left(-\frac{\partial \mathbf{P}}{\partial x}(x, y)\mathbf{A}^{-1}\right)\bar{\mathbf{q}}^{(e)}(t). \tag{47c}$$

The previous interpolations can be combined with those presented earlier in Eq. (13), permitting us to write:

$$\begin{Bmatrix} u_0^{(e)}(x, y, t) \\ v_0^{(e)}(x, y, t) \\ w_0^{(e)}(x, y, t) \\ \theta_x^{(e)}(x, y, t) \\ \theta_y^{(e)}(x, y, t) \end{Bmatrix} = \begin{bmatrix} N_1\mathbf{I}_2 & \mathbf{0}_{2\times3} & N_2\mathbf{I}_2 & \mathbf{0}_{2\times3} & N_3\mathbf{I}_2 & \mathbf{0}_{2\times3} & N_4\mathbf{I}_2 & \mathbf{0}_{2\times3} \\ \mathbf{0}_{1\times2} & \bar{\mathbf{N}}_{w,1}^{(e)} & \mathbf{0}_{1\times2} & \bar{\mathbf{N}}_{w,2}^{(e)} & \mathbf{0}_{1\times2} & \bar{\mathbf{N}}_{w,3}^{(e)} & \mathbf{0}_{1\times2} & \bar{\mathbf{N}}_{w,4}^{(e)} \\ \mathbf{0}_{1\times2} & \bar{\mathbf{N}}_{\theta_x,1}^{(e)} & \mathbf{0}_{1\times2} & \bar{\mathbf{N}}_{\theta_x,2}^{(e)} & \mathbf{0}_{1\times2} & \bar{\mathbf{N}}_{\theta_x,3}^{(e)} & \mathbf{0}_{1\times2} & \bar{\mathbf{N}}_{\theta_x,4}^{(e)} \\ \mathbf{0}_{3\times2} & \bar{\mathbf{N}}_{\theta_x,1}^{(e)} & \mathbf{0}_{1\times2} & \bar{\mathbf{N}}_{\theta_x,2}^{(e)} & \mathbf{0}_{1\times2} & \bar{\mathbf{N}}_{\theta_x,3}^{(e)} & \mathbf{0}_{1\times2} & \bar{\mathbf{N}}_{\theta_x,4}^{(e)} \end{bmatrix} \begin{Bmatrix} \mathbf{q}_1^{(e)}(t) \\ \mathbf{q}_2^{(e)}(t) \\ \mathbf{q}_3^{(e)}(t) \\ \mathbf{q}_4^{(e)}(t) \end{Bmatrix}, \tag{48}$$

where $\mathbf{q}_i^{(e)}(t) = \left\{u_{0,i}^{(e)}(t) \quad v_{0,i}^{(e)}(t) \quad w_{0,i}^{(e)}(t) \quad \theta_{x,i}^{(e)}(t) \quad \theta_{y,i}^{(e)}(t)\right\}^{\mathrm{T}}$ collects the DOFs related to node i, for $i \in \{1, 2, 3, 4\}$; $N_i = N_i(x, y)$ correspond to the interpolation functions introduced in Eq. (13); and $\mathbf{N}_{w,i}^{(e)}$, $\mathbf{N}_{\theta_x,i}^{(e)}$, $\mathbf{N}_{\theta_y,i}^{(e)}$ stand for 1×3 sub-matrices of $\mathbf{N}_w^{(e)}$, $\mathbf{N}_{\theta_x}^{(e)}$, $\mathbf{N}_{\theta_y}^{(e)}$, respectively, related to degrees of freedom of node i. For example, $\mathbf{N}_w^{(e)} = \left[\mathbf{N}_{w,1}^{(e)} \quad \mathbf{N}_{w,2}^{(e)} \quad \mathbf{N}_{w,3}^{(e)} \quad \mathbf{N}_{w,4}^{(e)}\right]$. Equation (48) can be rewritten as:

$$\begin{Bmatrix} u_0^{(e)}(x, y, t) \\ v_0^{(e)}(x, y, t) \\ w_0^{(e)}(x, y, t) \\ \theta_x^{(e)}(x, y, t) \\ \theta_y^{(e)}(x, y, t) \end{Bmatrix} = \begin{bmatrix} \mathbf{N}_u^{(e)}(x, y) \\ \mathbf{N}_v^{(e)}(x, y) \\ \mathbf{N}_w^{(e)}(x, y) \\ \mathbf{N}_{\theta_x}^{(e)}(x, y) \\ \mathbf{N}_{\theta_y}^{(e)}(x, y) \end{bmatrix} \mathbf{q}^{(e)}(t), \qquad \text{with} \qquad \mathbf{q}^{(e)}(t) = \begin{Bmatrix} \mathbf{q}_1^{(e)}(t) \\ \mathbf{q}_2^{(e)}(t) \\ \mathbf{q}_3^{(e)}(t) \\ \mathbf{q}_4^{(e)}(t) \end{Bmatrix} \tag{49}$$

and $\mathbf{N}_u^{(e)}$, $\mathbf{N}_v^{(e)}$, $\mathbf{N}_w^{(e)}$, $\mathbf{N}_{\theta_x}^{(e)}$, $\mathbf{N}_{\theta_y}^{(e)}$ corresponding to the rows of the interpolation matrix seen in Eq. (48).

2.2.3 Formulation at element level

The strains which are not identically equal to zero can be interpolated inside the domain of the FE now considered according to the relations:

$$\epsilon_x^{(e)}(x,y,z,t) = \left[\mathbf{B}_{x,0}^{(e)}(x,y) + z\mathbf{B}_{x,1}^{(e)}(x,y)\right]\mathbf{q}^{(e)}(t) = \left[\frac{\partial \mathbf{N}_u^{(e)}}{\partial x} - z\frac{\partial^2 \mathbf{N}_w^{(e)}}{\partial x^2}\right]\mathbf{q}^{(e)}(t); \tag{50a}$$

$$\epsilon_y^{(e)}(x,y,z,t) = \left[\mathbf{B}_{y,0}^{(e)}(x,y) + z\mathbf{B}_{y,1}^{(e)}(x,y)\right]\mathbf{q}^{(e)}(t) = \left[\frac{\partial \mathbf{N}_v^{(e)}}{\partial y} - z\frac{\partial^2 \mathbf{N}_w^{(e)}}{\partial y^2}\right]\mathbf{q}^{(e)}(t); \tag{50b}$$

$$\gamma_{xy}^{(e)}(x,y,z,t) = \left[\mathbf{B}_{xy,0}^{(e)}(x,y) + z\mathbf{B}_{xy,1}^{(e)}(x,y)\right]\mathbf{q}^{(e)}(t) = \left[\frac{\partial \mathbf{N}_u^{(e)}}{\partial y} + \frac{\partial \mathbf{N}_v^{(e)}}{\partial x} - 2z\frac{\partial^2 \mathbf{N}_w^{(e)}}{\partial x \partial y}\right]\mathbf{q}^{(e)}(t), \tag{50c}$$

which can be derived by combining Eqs. (49) and (44).

To showcase a situation in which the material of the plate does not exhibit linear isotropic behavior, here we consider the plate corresponds to a laminate, i.e. a collection of plies made of fibers, which are laid-up on top of one another, bonded with the aid of some resin, to produce a composite material. At this point, an important warning must be made by us, the authors: the adopted formulation, known as classical laminated plate theory, which copes with the Kirchhoff-Love plate theory, is the simplest available for performing analyzes of such structures. Hence, various results which might be derived (such as stresses and strains on individual plies) do not necessarily model reality with high fidelity. Other more advanced models do exist, such as equivalent single-layer theories that take into account shear deformations, and three-dimensional elasticity theories that model the laminate layers independently of one-another, while taking into account displacement compatibility between them (known as layerwise theories) [Reddy, 2003].

Having said this, the classical laminate theory can be used for simpler assessments. For the k-th lamina, stresses can be obtained using [Reddy, 2003]:

$$\begin{Bmatrix} \sigma_x^{(e)} \\ \sigma_y^{(e)} \\ \tau_{xy}^{(e)} \end{Bmatrix}^{(k)} = \begin{bmatrix} \bar{Q}_{11} & \bar{Q}_{12} & \bar{Q}_{16} \\ \bar{Q}_{12} & \bar{Q}_{22} & \bar{Q}_{26} \\ \bar{Q}_{16} & \bar{Q}_{26} & \bar{Q}_{66} \end{bmatrix}^{(k)} \begin{Bmatrix} \epsilon_x^{(e)} \\ \epsilon_y^{(e)} \\ \gamma_{xy}^{(e)} \end{Bmatrix}^{(k)} \quad \Leftrightarrow \quad \boldsymbol{\sigma}^{(e)} = \bar{\mathbf{Q}}^{(k)}\boldsymbol{\epsilon}^{(e)}, \quad \text{for } z_k \le z \le z_{k+1}, \tag{51}$$

where the superscript $^{(k)}$ appended to the vectors and matrix is used to indicate their entries are related to the k-th lamina of the laminate. The $\bar{Q}_{ij}^{(k)}$ components ($i,j \in \{1,2,6\}$) correspond to plane-stress reduced stiffnesses related to the material of the lamina, expressed in the global coordinate frame. They can be retrieved after performing a coordinate transformation of the material properties of the lamina, that is:

$$\bar{Q}_{11}^{(k)} = Q_{11}^{(k)}c_\alpha^4 + 2\left(Q_{12}^{(k)} + 2Q_{66}^{(k)}\right)s_\alpha^2c_\alpha^2 + Q_{22}^{(k)}s_\alpha^4; \tag{52a}$$

$$\bar{Q}_{12}^{(k)} = \left(Q_{11}^{(k)} + Q_{22}^{(k)} - 4Q_{66}^{(k)}\right)s_\alpha^2c_\alpha^2 + Q_{12}^{(k)}\left(s_\alpha^4 + c_\alpha^4\right); \tag{52b}$$

$$\bar{Q}_{22}^{(k)} = Q_{11}^{(k)}s_\alpha^4 + 2\left(Q_{12}^{(k)} + 2Q_{66}^{(k)}\right)s_\alpha^2c_\alpha^2 + Q_{22}^{(k)}c_\alpha^4; \tag{52c}$$

$$\bar{Q}_{16}^{(k)} = \left(Q_{11}^{(k)} - Q_{12}^{(k)} - 2Q_{66}^{(k)}\right)s_\alpha c_\alpha^3 + \left(Q_{12}^{(k)} - Q_{22}^{(k)} + 2Q_{66}^{(k)}\right)s_\alpha^3c_\alpha; \tag{52d}$$

$$\bar{Q}_{26}^{(k)} = \left(Q_{11}^{(k)} - Q_{12}^{(k)} - 2Q_{66}^{(k)}\right)s_\alpha^3c_\alpha + \left(Q_{12}^{(k)} - Q_{22}^{(k)} + 2Q_{66}^{(k)}\right)s_\alpha c_\alpha^3; \tag{52e}$$

$$\bar{Q}_{66}^{(k)} = \left(Q_{11}^{(k)} + Q_{22}^{(k)} - 2Q_{12}^{(k)} - 2Q_{66}^{(k)}\right)s_\alpha^2c_\alpha^2 + Q_{66}^{(k)}\left(s_\alpha^4 + c_\alpha^4\right). \tag{52f}$$

In these, $s_\alpha \coloneqq \sin\alpha^{(k)}$ and $c_\alpha \coloneqq \cos\alpha^{(k)}$, with $\alpha^{(k)}$ denoting the angle between the x principal direction of the k-th lamina with respect to the global x axis, cf. Fig. 8. The stiffnesses $Q_{ij}^{(k)}$ can be obtained from the engineering constants of the lamina, whose elastic behavior is assumed to be orthotropic:

$$Q_{11}^{(k)} = \frac{E_1^{(k)}}{1-\nu_{12}^{(k)}\nu_{21}^{(k)}}, \quad Q_{12}^{(k)} = \frac{\nu_{12}^{(k)}E_2^{(k)}}{1-\nu_{12}^{(k)}\nu_{21}^{(k)}} = \frac{\nu_{21}^{(k)}E_1^{(k)}}{1-\nu_{12}^{(k)}\nu_{21}^{(k)}}, \quad Q_{22}^{(k)} = \frac{E_2^{(k)}}{1-\nu_{12}^{(k)}\nu_{21}^{(k)}}, \quad Q_{66}^{(k)} = G_{12}^{(k)}. \tag{53}$$

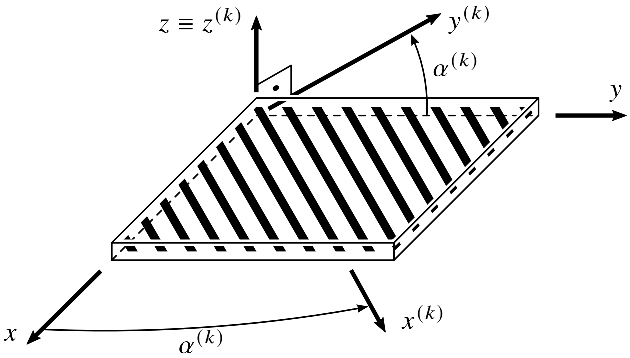

Figure 8: Principal coordinate system $x^{(k)}y^{(k)}z^{(k)}$ related to an uni-directional ply of a laminate, whose orientation with respect to the global reference frame xyz is given by $\alpha^{(k)}$.

With the previous expressions at hand, we can obtain the kinetic and potential energies necessary for establishing the finite element matrices, when the variational formulation approach is used. For the kinetic energy, we have:

$$\begin{aligned}
\mathcal{K}^{(e)} &= \iiint_{\Omega_t^{(e)}} \frac{1}{2}\rho^{(e)} \left\{ \left[\dot{u}^{(e)}(x,y,z,t)\right]^2 + \left[\dot{v}^{(e)}(x,y,z,t)\right]^2 + \left[\dot{w}^{(e)}(x,y,z,t)\right]^2 \right\} \mathrm{d}x\,\mathrm{d}y\,\mathrm{d}z \\
&= \sum_{k=1}^{N_\text{layers}} \int_{z_k}^{z_{z+1}} \int_{-b}^{b} \int_{-a}^{a} \frac{1}{2}\rho^{(e)} \left\{ \left[\dot{u}^{(e)}(x,y,z,t)\right]^2 \right. \\
&\qquad\qquad \left. + \left[\dot{v}^{(e)}(x,y,z,t)\right]^2 + \left[\dot{w}^{(e)}(x,y,z,t)\right]^2 \right\} \mathrm{d}x\,\mathrm{d}y\,\mathrm{d}z \\
&= \sum_{k=1}^{N_\text{layers}} \int_{z_k}^{z_{z+1}} \int_{-b}^{b} \int_{-a}^{a} \frac{1}{2}\rho^{(e)} \left\{ \dot{\mathbf{q}}^{(e)\mathrm{T}} \left(\mathbf{N}_u^{(e)} + z\mathbf{N}_{\theta_y}^{(e)}\right)^\mathrm{T} \left(\mathbf{N}_u^{(e)} + z\mathbf{N}_{\theta_y}^{(e)}\right) \dot{\mathbf{q}}^{(e)} \right. \\
&\qquad \left. + \dot{\mathbf{q}}^{(e)\mathrm{T}} \left(\mathbf{N}_v^{(e)} - z\mathbf{N}_{\theta_x}^{(e)}\right)^\mathrm{T} \left(\mathbf{N}_v^{(e)} - z\mathbf{N}_{\theta_x}^{(e)}\right) \dot{\mathbf{q}}^{(e)} + \dot{\mathbf{q}}^{(e)\mathrm{T}} \mathbf{N}_w^{(e)\mathrm{T}} \mathbf{N}_w^{(e)} \dot{\mathbf{q}}^{(e)} \right\} \mathrm{d}x\,\mathrm{d}y\,\mathrm{d}z \\
&= \frac{1}{2}\dot{\mathbf{q}}^{(e)\mathrm{T}} \left[\sum_{k=1}^{N_\text{layers}} \int_{z_k}^{z_{z+1}} \int_{-b}^{b} \int_{-a}^{a} \rho^{(e)} \left\{ \left(\mathbf{N}_u^{(e)} + z\mathbf{N}_{\theta_y}^{(e)}\right)^\mathrm{T} \left(\mathbf{N}_u^{(e)} + z\mathbf{N}_{\theta_y}^{(e)}\right) \right. \right. \\
&\qquad \left. \left. + \left(\mathbf{N}_v^{(e)} - z\mathbf{N}_{\theta_x}^{(e)}\right)^\mathrm{T} \left(\mathbf{N}_v^{(e)} - z\mathbf{N}_{\theta_x}^{(e)}\right) + \mathbf{N}_w^{(e)\mathrm{T}} \mathbf{N}_w^{(e)} \right\} \mathrm{d}x\,\mathrm{d}y\,\mathrm{d}z \right] \dot{\mathbf{q}}^{(e)} \\
&= \frac{1}{2}\dot{\mathbf{q}}^{(e)\mathrm{T}} \left[\sum_{k=1}^{N_\text{layers}} \int_{z_k}^{z_{z+1}} \int_{-b}^{b} \int_{-a}^{a} \rho^{(e)} \left\{ \mathbf{N}_u^{(e)\mathrm{T}} \mathbf{N}_u^{(e)} + z\left(\mathbf{N}_{\theta_y}^{(e)\mathrm{T}} \mathbf{N}_u^{(e)} + \mathbf{N}_u^{(e)\mathrm{T}} \mathbf{N}_{\theta_y}^{(e)}\right) \right. \right. \\
&\qquad + z^2 \mathbf{N}_{\theta_y}^{(e)\mathrm{T}} \mathbf{N}_{\theta_y}^{(e)} + \mathbf{N}_v^{(e)\mathrm{T}} \mathbf{N}_v^{(e)} - z\left(\mathbf{N}_{\theta_x}^{(e)\mathrm{T}} \mathbf{N}_v^{(e)} + \mathbf{N}_v^{(e)\mathrm{T}} \mathbf{N}_{\theta_x}^{(e)}\right) \\
&\qquad \left. \left. + z^2 \mathbf{N}_{\theta_x}^{(e)\mathrm{T}} \mathbf{N}_{\theta_x}^{(e)} + \mathbf{N}_w^{(e)\mathrm{T}} \mathbf{N}_w^{(e)} \right\} \mathrm{d}x\,\mathrm{d}y\,\mathrm{d}z \right] \dot{\mathbf{q}}^{(e)} \\
&= \frac{1}{2}\dot{\mathbf{q}}^{(e)\mathrm{T}}(t) \left[\sum_{k=1}^{N_\text{layers}} \mathbf{M}^{(e)\,(k)} \right] \dot{\mathbf{q}}^{(e)}(t) = \frac{1}{2}\dot{\mathbf{q}}^{(e)\mathrm{T}}(t) \mathbf{M}^{(e)} \dot{\mathbf{q}}^{(e)}(t),
\end{aligned} \tag{54}$$

where:

$$\mathbf{M}^{(e)\,(k)} = (z_{k+1} - z_k)\int_{-b}^{b}\int_{-a}^{a}\rho^{(e)\,(k)}\left(\mathbf{N}_u^{(e)\,\mathrm{T}}\mathbf{N}_u^{(e)} + \mathbf{N}_v^{(e)\,\mathrm{T}}\mathbf{N}_v^{(e)} + \mathbf{N}_w^{(e)\,\mathrm{T}}\mathbf{N}_w^{(e)}\right)\mathrm{d}x\,\mathrm{d}y$$
$$+ \frac{1}{2}\left(z_{k+1}^2 - z_k^2\right)\int_{-b}^{b}\int_{-a}^{a}\rho^{(e)\,(k)}\left(\mathbf{N}_{\theta_y}^{(e)\,\mathrm{T}}\mathbf{N}_u^{(e)} + \mathbf{N}_u^{(e)\,\mathrm{T}}\mathbf{N}_{\theta_y}^{(e)} - \mathbf{N}_{\theta_x}^{(e)\,\mathrm{T}}\mathbf{N}_v^{(e)} - \mathbf{N}_v^{(e)\,\mathrm{T}}\mathbf{N}_{\theta_x}^{(e)}\right)\mathrm{d}x\,\mathrm{d}y$$
$$+ \frac{1}{3}\left(z_{k+1}^3 - z_k^3\right)\int_{-b}^{b}\int_{-a}^{a}\rho^{(e)\,(k)}\left(\mathbf{N}_{\theta_y}^{(e)\,\mathrm{T}}\mathbf{N}_{\theta_y}^{(e)} + \mathbf{N}_{\theta_x}^{(e)\,\mathrm{T}}\mathbf{N}_{\theta_x}^{(e)}\right)\mathrm{d}x\,\mathrm{d}y \quad (55)$$

corresponds to the mass matrix contribution owed to the k-th layer of the laminate. The total mass matrix of the plate/laminate finite element is obtained by summing the contributions of all its laminas:

$$\mathbf{M}^{(e)} = \sum_{k=1}^{N_\text{layers}}\mathbf{M}^{(e)\,(k)}. \quad (56)$$

With regards to the contribution due to elastic deformation of the structure towards the finite element potential energy, it can be obtained from:

$$\begin{aligned}
\mathcal{U}_\text{elast}^{(e)} &= \frac{1}{2}\iiint_{\Omega_t^{(e)}}\left[\sigma_x^{(e)}\epsilon_x^{(e)} + \sigma_y^{(e)}\epsilon_y^{(e)} + \tau_{xy}^{(e)}\gamma_{xy}^{(e)}\right]\mathrm{d}x\,\mathrm{d}y\,\mathrm{d}z \\
&= \frac{1}{2}\sum_{k=1}^{N_\text{layers}}\int_{z_k}^{z_{z+1}}\int_{-b}^{b}\int_{-a}^{a}\boldsymbol{\sigma}^{(e)\,\mathrm{T}}(x,y,z,t)\boldsymbol{\epsilon}^{(e)}(x,y,z,t)\,\mathrm{d}x\,\mathrm{d}y\,\mathrm{d}z \\
&= \frac{1}{2}\mathbf{q}^{(e)\,\mathrm{T}}(t)\left[\sum_{k=1}^{N_\text{layers}}\int_{z_k}^{z_{z+1}}\int_{-b}^{b}\int_{-a}^{a}\left(\mathbf{B}_0^{(e)} + z\mathbf{B}_1^{(e)}\right)^\mathrm{T}\bar{\mathbf{Q}}^{(k)}\left(\mathbf{B}_0^{(e)} + z\mathbf{B}_1^{(e)}\right)\mathrm{d}x\,\mathrm{d}y\,\mathrm{d}z\right]\mathbf{q}^{(e)}(t) \\
&= \frac{1}{2}\mathbf{q}^{(e)\,\mathrm{T}}(t)\left[\sum_{k=1}^{N_\text{layers}}\mathbf{K}^{(e)\,(k)}\right]\mathbf{q}^{(e)}(t) = \frac{1}{2}\mathbf{q}^{(e)\,\mathrm{T}}(t)\mathbf{K}^{(e)}\mathbf{q}^{(e)}(t), \quad (57)
\end{aligned}$$

where $\mathbf{K}^{(e)\,(k)}$ is the stiffness matrix contribution due to the k-th layer of the laminate, whose expression is given by:

$$\mathbf{K}^{(e)\,(k)} = (z_{k+1} - z_k)\int_{-b}^{b}\int_{-a}^{a}\mathbf{B}_0^{(e)\,\mathrm{T}}\bar{\mathbf{Q}}^{(k)}\mathbf{B}_0^{(e)}\mathrm{d}x\,\mathrm{d}y$$
$$+ \frac{1}{2}\left(z_{k+1}^2 - z_k^2\right)\int_{-b}^{b}\int_{-a}^{a}\left(\mathbf{B}_1^{(e)\,\mathrm{T}}\bar{\mathbf{Q}}^{(k)}\mathbf{B}_0^{(e)} + \mathbf{B}_0^{(e)\,\mathrm{T}}\bar{\mathbf{Q}}^{(k)}\mathbf{B}_1^{(e)}\right)\mathrm{d}x\,\mathrm{d}y$$
$$+ \frac{1}{3}\left(z_{k+1}^3 - z_k^3\right)\int_{-b}^{b}\int_{-a}^{a}\mathbf{B}_1^{(e)\,\mathrm{T}}\bar{\mathbf{Q}}^{(k)}\mathbf{B}_1^{(e)}\mathrm{d}x\,\mathrm{d}y. \quad (58)$$

In the previous developments, we have made use of matrices $\mathbf{B}_0^{(e)}$ and $\mathbf{B}_1^{(e)}$, which are employed for interpolating the strain vector $\boldsymbol{\epsilon}^{(e)}$ inside the finite element domain. They can be evaluated using:

$$\mathbf{B}_0^{(e)} = \begin{bmatrix}\mathbf{B}_{x,0}^{(e)} \\ \mathbf{B}_{y,0}^{(e)} \\ \mathbf{B}_{xy,0}^{(e)}\end{bmatrix} \qquad \text{and} \qquad \mathbf{B}_1^{(e)} = \begin{bmatrix}\mathbf{B}_{x,1}^{(e)} \\ \mathbf{B}_{y,1}^{(e)} \\ \mathbf{B}_{xy,1}^{(e)}\end{bmatrix}, \quad (59)$$

with entries being implicitly defined in Eq. (50). The complete finite element stiffness matrix can then be obtained via:

$$\mathbf{K}^{(e)} = \sum_{k=1}^{N_\text{layers}}\mathbf{K}^{(e)\,(k)}. \quad (60)$$

As for conservative external loads which can be applied to the finite element, their contribution can be obtained following similar steps to those which have led to Eq. (28) in the previous section. Here, we simply consider that:

$$\mathcal{W}_\text{ext}^{(e)} = \mathbf{q}^{(e)\,\mathrm{T}}(t)\mathbf{Q}_b^{(e)}(t) + \mathbf{q}^{(e)\,\mathrm{T}}(t)\mathbf{Q}_s^{(e)}(t), \quad (61)$$

without going into details, or providing expressions that result for the element body and surface forces, $\mathbf{Q}_b^{(e)}(t)$ and $\mathbf{Q}_s^{(e)}(t)$, respectively.

At this point, we are able to evaluate the finite element Lagrangian, which takes the same form seen in Eq. (35), albeit expressions for the element mass and stiffness matrices, as well as conservative load vectors resulted different. The equations of motion for the plate/laminate finite element can also be established, and look exactly like what has been presented in Eq. (37) — but with $\mathbf{M}^{(e)}$ and $\mathbf{K}^{(e)}$ given by Eqs. (56) and (60), for example.

Finally, the procedure outlined in the previous section for obtaining global matrices for a finite element mesh can be easily generalized to account for finite elements with any number of DOFs. Henceforth, it can be readily used to establish global matrices related to a mesh assembled using plate/laminate elements, such as the one just presented.

3 Examples

In order to showcase the use of the finite elements whose mathematical formulation has been discussed previously in section 2, in this section we consider two relatively simple examples. The first one makes use of the quadrilateral two-dimensional elasticity finite element presented in section 2.1, whilst the second example concerns itself with the rectangular laminate finite element introduced in section 2.2. Numerical codes used to perform computations have been implemented in MATLAB ® by the authors, and are made publicly available through this link.

3.1 Static analysis of an H-shaped material sheet

Problem: Consider a H-shaped sheet, clamped at its left edge and subjected to a distributed load $q(x)$ at its top-right portion, as illustrated in Fig. 9. The structure is made up of an isotropic metallic material and its physical and geometric properties are listed in Tab. 1. By employing quadrilateral two-dimensional elasticity finite elements, let us estimate the stress and strain fields distribution in the sheet domain.

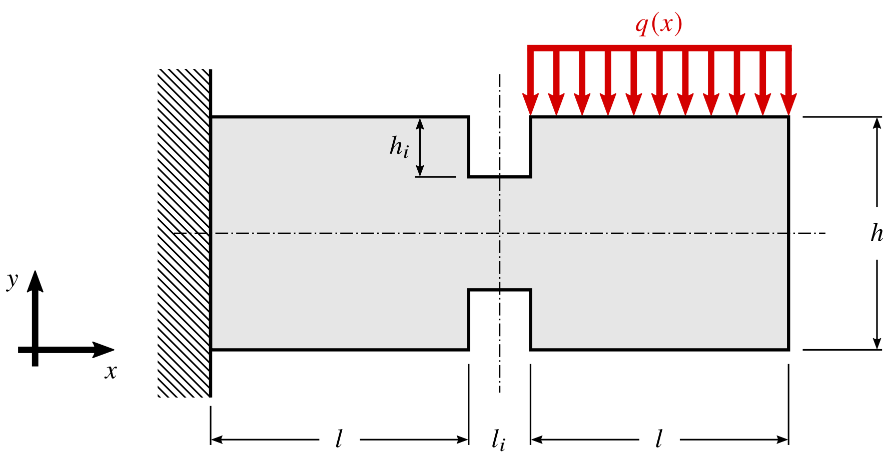

Figure 9: H-shaped sheet clamped at its left edge and subjected to a vertical distributed load on part of its boundary.

Table 1: H-shaped sheet dimensions and material properties.

Variable	Description	Value	Units
l_t	Total length	1	m
l	Length of first and third sections	0.4	m
l_i	Length of intermediate section	0.2	m
h	Total height	0.4	m
h_i	Height of the intermediate cutout	60	mm
L_z	Thickness along z	5	mm
E	Young's modulus	69	GPa
ν	Poisson's ratio	0.3	
ρ	Mass density	2.7	$\mathrm{g\,m^{-3}}$

Solution: Considering that the thickness of the solid medium is negligible in comparison to its other dimensions, and that stresses are confined to the sheet plane, only, the Solid Mechanics problem at hand consists of a plane stress one.

As previously mentioned in section 2.1.2, for plane stress problems, the nonzero stresses are σ_x, σ_y and τ_{xy}, if the solid sheet is located on the x-y plane. For this scenario, considering linear, isotropic elasticity, Hooke's law, stated in Eqs. (7), can be duly modified, to provide a reduced set of constitutive relations, cf. Eqs. (24).

The first step which must be made to obtain the desired stress distributions using the FEM is to define the mesh for the domain of the considered sheet. For this purpose, we make use of the quadrilateral two-dimensional continuum elasticity finite element presented in section 2.1. One recalls that, for this element, the nodal DOFs comprise displacements, only, and that its interpolation functions are linear for displacements.

In order to better organize the mesh, the domain of the H-shaped sheet is divided in seven rectangular sub-regions, as illustrated in Fig. 10. This makes it more straightforward to establish the number of finite elements and the location of nodes, in such a way that rectangular elements are used to make a mapped mesh for the whole domain.

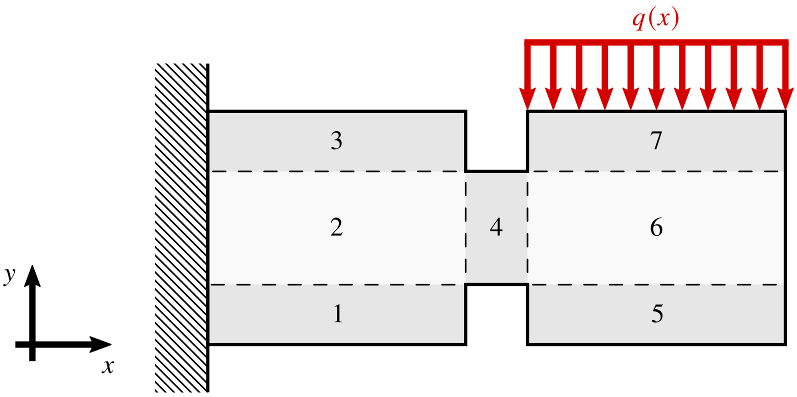

Figure 10: Division of the H-shaped sheet into seven rectangular sub-domains.

One then has to ensure that edges shared by neighbour rectangular sub-domains have the same amount of nodes. Besides simplifying the generation of a mapped mesh, this reasoning facilitates adequately coupling the motion of sub-domains which are neighbors, for which meshes are initially generated independently of one another. This coupling can be made by enforcing the same nodal DOFs for distinct nodes, which is essentially the same as merging the coincident nodes, at this setting. More complicated coupling of sub-domains is also possible, taking into account *constraint equations*, which can be enforced via Lagrange multipliers or penalty methods [Bathe, 2014]. For the example at hand, for the correct link between nodes of the rectangular sub-domains, one must abide by the following pattern for the number of elements for the edges of the rectangular partitions:

- Edges parallel to the x direction of rectangles 1, 2 and 3 must have the same number of elements;
- Edges parallel to the y direction of rectangles 2, 4 and 6 must have the same number of elements;
- Edges parallel to the x direction of rectangles 5, 6 and 7 must have the same number of elements.

Given the above, one must now choose the number of finite elements (and consequently, nodes) that will compose the mesh. In general terms, the accuracy of the result tends to improve as the mesh gets refined, because the interpolation of field variables inside the domain of a finite element becomes more and more representative of the actual solution. On the other hand, as consequence of reducing the size of elements, the cost of computational simulations, in terms of resources and time, increases as well. In these terms, sometimes it becomes necessary to adopt a compromise solution, since the computational cost to perform various simulations with a mesh comprising a large number of elements can be prohibitive. Several authors, e.g. [Zienkiewicz et al., 2013], propose performing *convergence analysis* of the mesh, based on the results which are sought, in order to find a reasonable cost-benefit ratio for the mesh employed for numerical simulations; or to assure that results are independent of the mesh, i.e. that they have converged to the actual solution of the problem at hand.

In order to highlight the importance of a suitable specification for a finite element mesh, the example one is considering has been resolved for two different meshes, made of elements with distinct sizes:

- **Case 1:** the element size (length and height) is 5% of the largest dimension (50 mm, for this problem).
- **Case 2:** the element size (length and height) is 1% of the largest dimension (10 mm, for this problem).

Accordingly, the number of divisions used for the edges of each rectangular sub-domain, along the x and y directions, $n_{ele\,x}$ and $n_{ele\,y}$, respectively, is presented in Tab. 2. Additionally, Tab. 3 shows some statistics of the resulting meshes, such as the total number of elements, nodes and DOFs. The meshes associated with Cases 1 and 2 are presented in Figs. 11(a) and 11(b), respectively, by means of the location occupied by nodes. By comparing both figures, it is clear that reducing the finite element size by 5 times (Case 1 to Case 2) implies in a much denser mesh.

As explained in section 2.1.1, the quadrilateral finite element used for this problem has four nodes, and two DOFs per node (displacements u and v along the x and y directions, respectively). Accordingly, the total number of DOFs related to the mesh associated with Case 2 increases significantly in comparison to the one observed for Case 1. Furthermore, the time spent to perform computations increases substantially, as well, as can be seen from the last row presented in Tab. 3. One should clarify that the reported times have been measured for a laptop computer, running Microsoft Windows 10 operating system, equipped with an Intel® Core™ i7-6500U central processing unit, and 8 GB of RAM memory.

Table 2: Number of elements along x and y directions adopted for each of the rectangular sub-domains identified in Fig. 10.

Rectangle number	Case 1		Case 2	
	n_{ele_x}	n_{ele_y}	n_{ele_x}	n_{ele_y}
1	8	2	40	7
2	8	6	40	28
3	8	2	40	7
4	4	6	20	28
5	8	5	40	7
6	8	6	40	28
7	8	7	40	7

Table 3: Statistics related to the meshes obtained for the H-shaped sheet considered in this example.

Statistic	Case 1	Case 2
Total number of elements	184	3920
Total number of nodes	269 (219)†	4299 (4077)†
Total number of DOFs	538 (438)†	8598 (8154)†
Elapsed time [s]	9.1	433.1

† Values reported between parentheses are related to the number of nodes and DOFs after coincident entities were merged.

It is important to note that, after the initial mesh has been generated individually for each rectangular sub-domain, some overlapping nodes could be found. “Duplicated” and “triplicated” nodes were then eliminated, to ensure the continuity of the finite element mesh. Underlying data of the finite element mesh model also need to be taken care of during this process. For example, various information are encoded in matrices used in finite element codes, related to properties of elements and nodes, and are therefore affected when nodes and DOFs get merged together. In this regard, in our code, some prominent matrices are:

- the “node matrix”, which stores information about which nodes are related to each element;
- the “node position matrix”, which caches the location initially occupied by nodes;
- the “connectivity matrix”, which stores which DOFs are related to each element.

Hence, after coincident nodes are dealt with, these matrices are properly adjusted. One should remark that, to facilitate further operations, such as assembling global matrices, nodes and DOFs can be renumbered, if desired.

After nodes and DOFs have been updated, one has to input what are the boundary conditions. For this purpose, the nodes which are located on the boundary of the H-shaped sheet are identified. The DOFs related to those nodes at the left must be enforced to be zero. (A mathematical procedure which can be used for this purpose is presented in our next example, in section 3.2.) With regards to those elements at the top of rectangle 7, one has to impose a distributed pressure load, $q(x) = 500\,\text{kPa}$, to their appropriate boundary/edge, cf. Eq. (32). All other segments that compose the boundary of the structure are free. In Figs. 12(a) and 12(b), it is possible to visualize

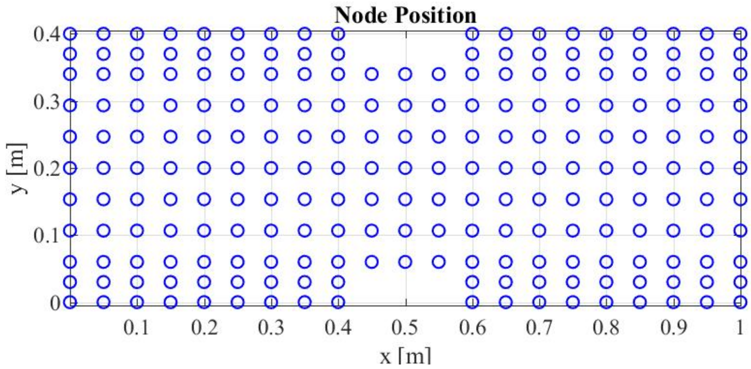

(a) Case 1

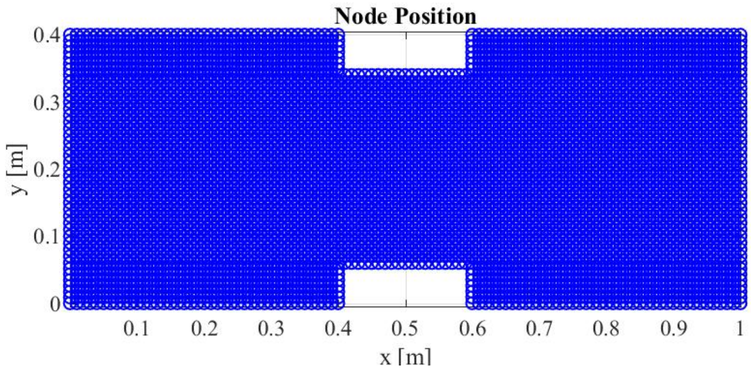

(b) Case 2

Figure 11: Location of nodes that compose the meshes of the H-shaped sheet of this example.

which nodes are related to each type of boundary condition just described, i.e. those which are totally blocked/restrained, related to the distributed pressure load, and/or free to move, without externally applied loads.

With boundary conditions defined, element level matrices can be computed (cf. Eqs. (27) and (34)) and global level matrices assembled (cf. Eq. (40)). The external distributed, surface load contribution can be evaluated by resorting to Eqs. (32) and (41). Having calculated global matrices and vectors, one can resolve a linear system of equations to determine the nodal DOFs of the mesh. This corresponds to a static analysis of the considered structure. The equations which needs to be solved come directly from Eq. (42) — one only needs to disregard the inertia/mass contribution term on its left-hand side to arrive at the appropriate global level input-output relationship for the analyzed system.

Figures 13(a) and 13(b) show how nodes get displaced when the H-shaped sheet is solicited by the external pressure load, for the two different meshes which we are considering. For Case 1, the largest displacement value occurs for the node at the top-right vertex of the sheet (with coordinates $x = 1$ m, $y = 0.4$ m), being its value equal to 0.199 27 mm. For Case 2, the maximum displacement is 0.205 449 mm, occurring at the same location observed for the previous case. To make for a better visualization of the displacement results, in Figs. 13(a) and 13(b) one has used amplification factors, whose values have been automatically computed, based on a characteristic dimension of the sheet and the maximum node displacement.

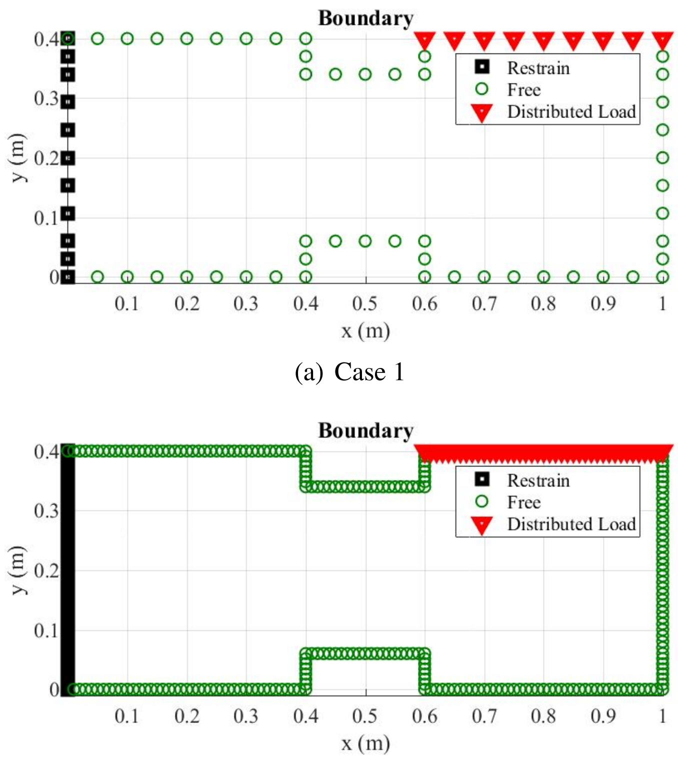

(a) Case 1

(b) Case 2

Figure 12: Boundary conditions implemented for analyzing the H-shaped sheet considered in this example.

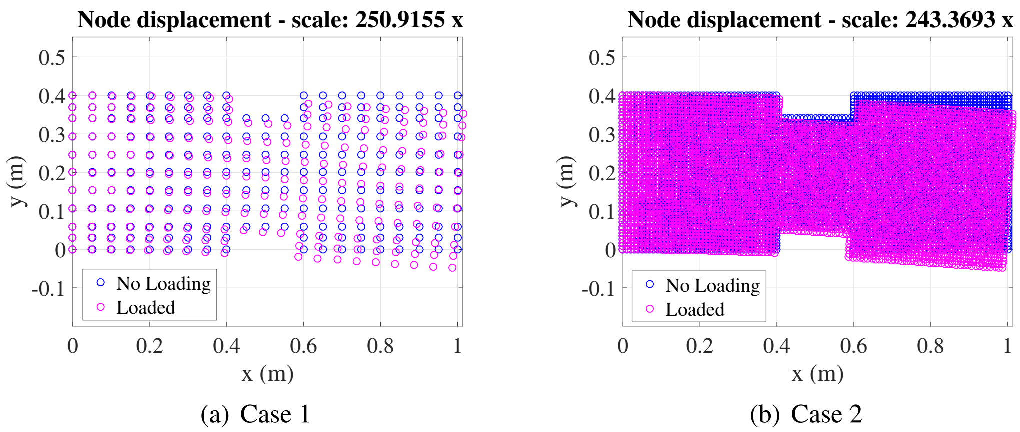

(a) Case 1 (b) Case 2

Figure 13: Node displacements resulting for the H-shaped sheet considered in this example.

With the complete nodal DOFs' vector being calculated, stress and strain results can be established via post-processing, for each element of the mesh. The displacements related to the nodes of an element can be initially obtained by considering the element DOFs' localization matrix, cf. (38). The strains can then be evaluated with the help of the element strain-displacement matrix $\mathbf{B}^{(e)}$, cf. Eq. (23). Stresses can then be retrieved by recalling the material constitutive relations, cf. Eq. (24) in the present case. Taking into account that strains and stresses vary linearly inside the domain of each finite element of the mesh, due to the element formulation, one can establish the plots shown in Figs. 14 and 15 for Cases 1 and 2, respectively.

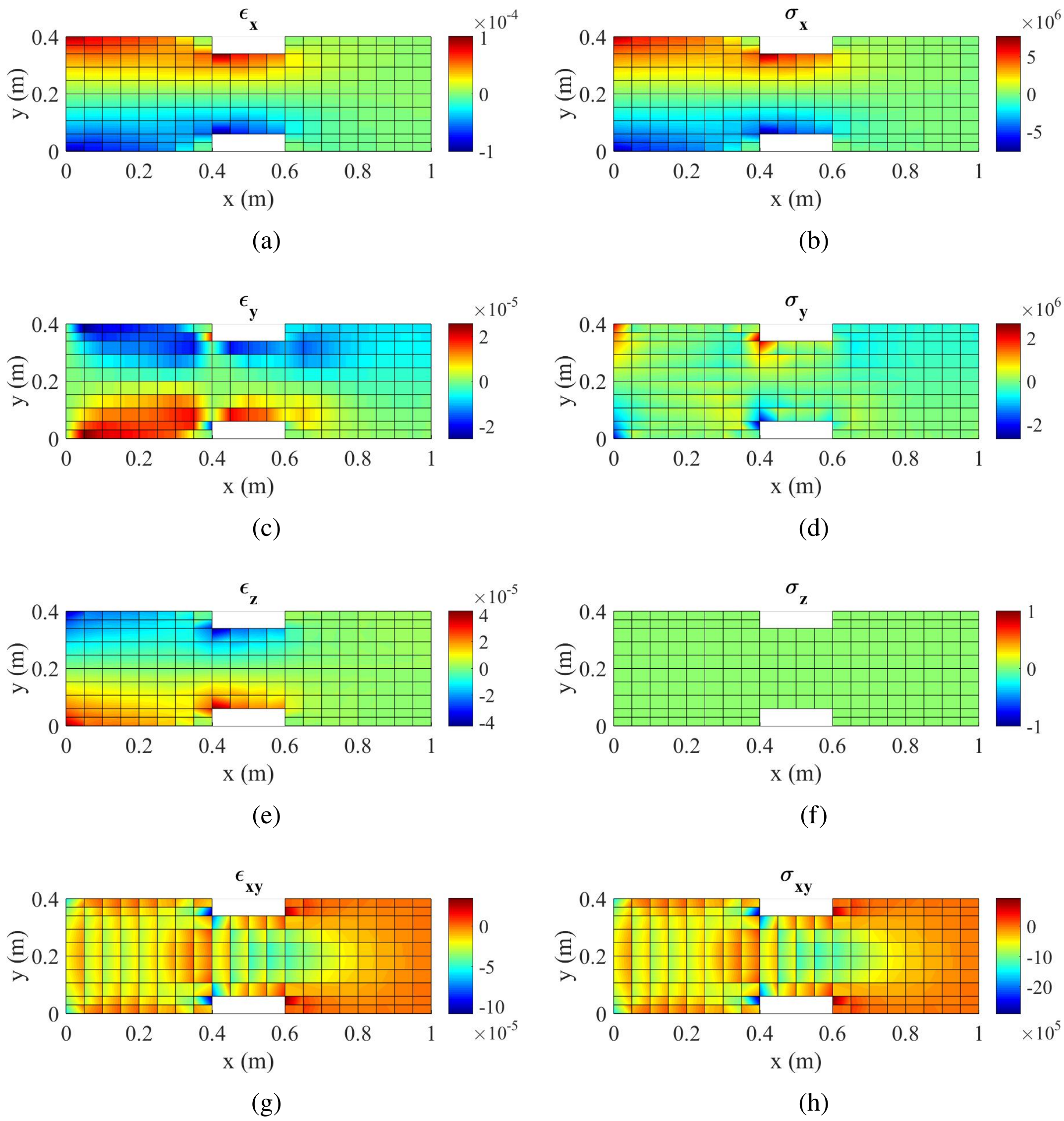

Figure 14: Distributions of strains and stresses in the H-shaped sheet considered in this example, using the coarser mesh of Case 1.

Regarding the maximum and minimum values observed for stresses and strains, σ_x reaches its maximum at the left internal corner of the top cutout, precisely at coordinates $x = 0.4$ m, $y = 0.34$ m. The minimum value of σ_x occurs at the equivalent place of the bottom cutout, at $x = 0.4$ m, $y = 0.06$ m, as expected for this configuration. The behavior of the normal strain ϵ_x is very similar, which is in accordance with the constitutive relation (24). For the normal stress and strain along the y direction (σ_y, ϵ_y), maximum and minimum values are seen at the same locations. With regards to the out-of-plane strain ϵ_z, it takes extrema values in the same cutouts, but in this case the maximum is seen to happen in the bottom location, whilst the minimum ϵ_z strain happens at the left internal corner of the top cutout. The stress σ_z is always zero, in accordance with the hypothesis if plane stress behavior.

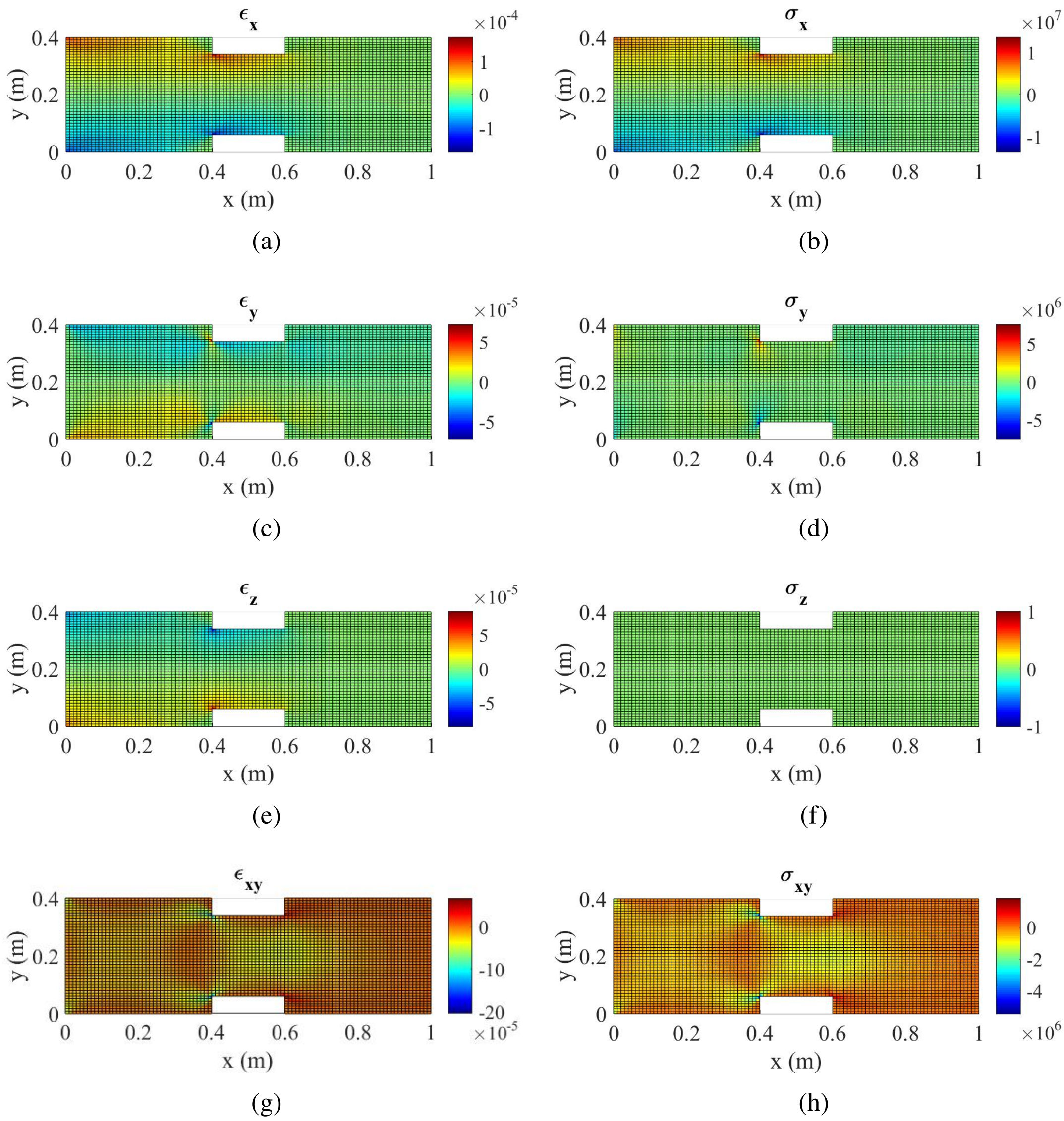

Figure 15: Distributions of strains and stresses in the H-shaped sheet considered in this example, using the finer mesh of Case 2.

Table 4: Comparison of the results obtained for the H-shaped sheet using the two generated meshes, in terms of the calculated maximum stresses.

	Case 1		Case 2	
	$\sigma_{\max}$ [MPa]	(x, y) [m]	$\sigma_{\max}$ [MPa]	(x, y) [m]
σ_x	7.6902	(0.40,0.34)	13.7456	(0.40,0.34)
σ_y	2.6720	(0.40,0.34)	7.5453	(0.40,0.34)
τ_{xy}	0.9190	(0.60,0.06)	1.7960	(0.60,0.06)

Table 5: Comparison of the results obtained for the H-shaped sheet using the two generated meshes, in terms of the calculated minimum stresses.

	Case 1		Case 2	
	$\sigma_{\min}$ [MPa]	(x, y) [m]	$\sigma_{\min}$ [MPa]	(x, y) [m]
σ_x	−7.6465	(0.40,0.06)	−13.7084	(0.40,0.06)
σ_y	−2.6692	(0.40,0.06)	−7.5453	(0.40,0.06)
τ_{xy}	−2.8987	(0.40,0.34)	−5.4430	(0.40,0.34)

From the results obtained for the maximum and minimum stresses, which are reported in Tabs. 4 and 5, respectively, it becomes clear that the values for the stresses obtained with the coarser (Case 1) and finer (Case 2) meshes are quite different between themselves. This is specially true because the analyzed structure has cutouts with right angle corners, which act as stress risers. For this, if one wants to obtain a better convergence of stress results using the four-nodes, quadrilateral, two-dimensional elasticity finite elements, it is necessary to develop a more complex mesh, using finer discretization, specially at the locations where stress concentration is expected to occur.

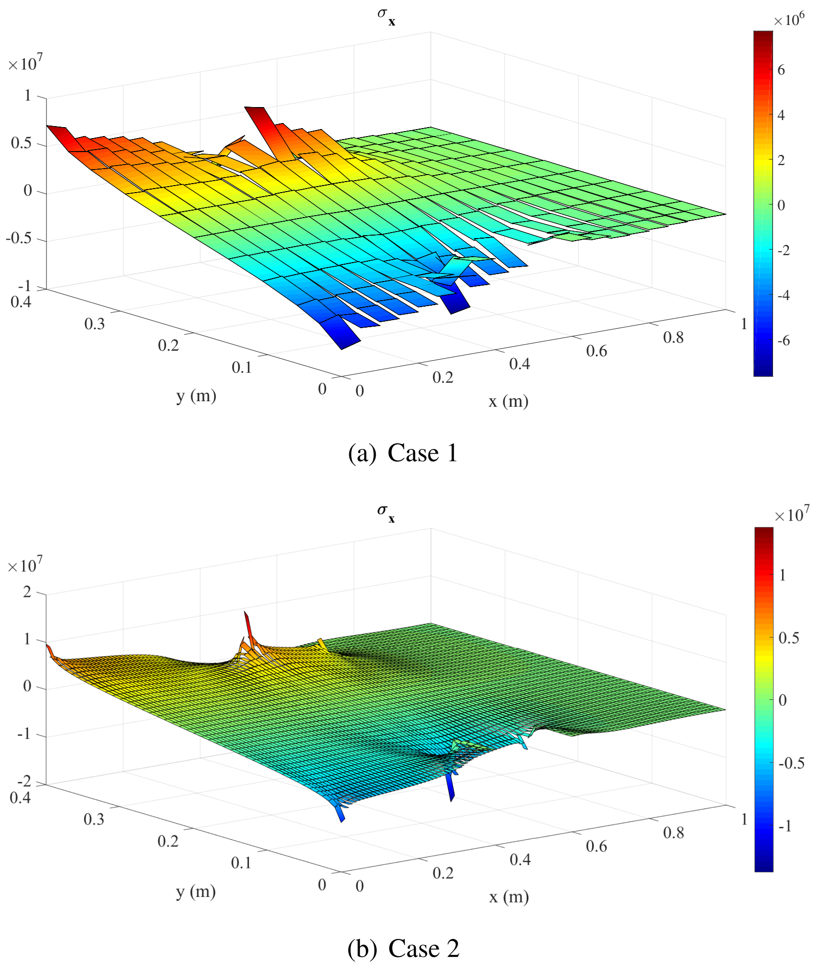

Figure 16: Three-dimensional visualization of the σ_x stress field for Cases 1 and 2 related to the H-shaped sheet considered in this example.

To help enlighten this remark, three-dimensional views are presented in Fig. 16 for the σ_x normal stress field, for both considered meshes. In Fig. 16(a), it is possible to see that the shown stress result has various discontinuities between adjacent finite elements, even at shared nodes. This is a clear indication that the considered stress result has not converged to the true solution of the problem, indicating that further mesh refinement should be considered; or that another type of finite element should be used, to provide better interpolation capability. When the three-dimensional visualization shown in Fig. 16(b) is considered, then fewer discontinuities are seen, and those which are related to significant jumps in value are confined exclusively to right angle corners at the cutouts and at the clamped region. If Saint-Venant's principle is invoked [Fung et al., 2017], then the computed results are reasonably representative of the actual solution of the Solid Mechanics problem at hand, except at the stress concentration regions just identified. Similar observations can be made if one analyzes the three-dimensional plots depicted in Fig. 17 for ϵ_y.

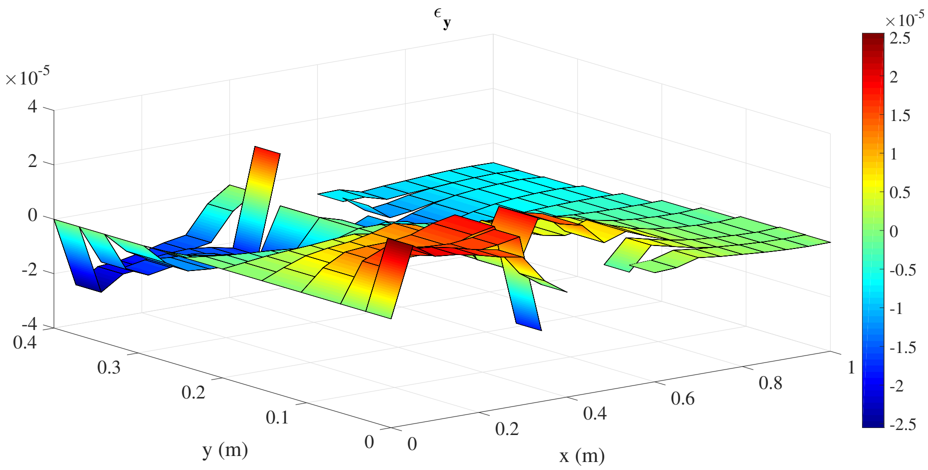

(a) Case 1

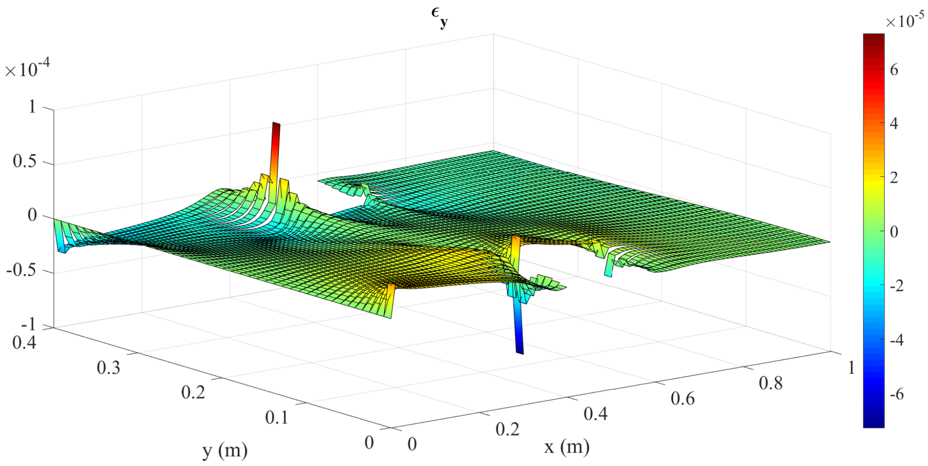

(b) Case 2

Figure 17: Three-dimensional visualization of the ϵ_y strain field for Cases 1 and 2 related to the H-shaped sheet considered in this example.

3.2 Dynamic analysis of a rectangular laminate

As a second example, now we consider a rectangular laminate, as illustrated in Fig. 18. It has dimensions $a = 287$ mm and $b = 287$ mm, being composed of four layers with individual thickness $h^{(k)} = 0.184$ mm, for $k \in \{1, 2, 3, 4\}$. The orientation of the layers is such that $\alpha^{(k)} = (-1)^k 45°$. Additionally, each layer is made of HexPly® M21/IM7, for which $E_1 = 160\,\text{GPa}$, $E_2 = 8.6\,\text{GPa}$, $\nu_{12} = 0.31$, $G_{12} = 4.7\,\text{GPa}$, $\rho = 1580\,\text{kg}\,\text{m}^{-3}$ [Pereira et al., 2020]. The laminate is clamped on one of its sides, located at $x = 0$, as shown.

Based on the global level equations of motion for the considered system, which read:

$$\mathbf{M}^{(g)}\ddot{\mathbf{q}}^{(g)}(t) + \mathbf{K}^{(g)}\mathbf{q}^{(g)}(t) = \mathbf{Q}^{(g)}(t), \tag{62}$$

different types of dynamic analyzes can be made. Here, $\mathbf{Q}^{(g)}$ corresponds to a vector of arbitrary external forces. Furthermore, depending on the dynamic analysis which is of interest, initial conditions must be provided, in the form of initial displacements $\mathbf{q}_0^{(g)}$ and initial velocities $\dot{\mathbf{q}}_0^{(g)}$.

To take into account the clamp boundary condition, or other ones, which can be explicitly written in terms of the global nodal DOFs vector $\mathbf{q}^{(g)}(t)$, we partition it in unconstrained (free) and constrained subsets, such that:

$$\mathbf{q}^{(g)}(t) = \begin{Bmatrix} \mathbf{q}_u^{(g)}(t) \\ \mathbf{q}_c^{(g)}(t) \end{Bmatrix}. \tag{63}$$

For the considered case, all DOFs related to nodes located on the clamped edge are included in $\mathbf{q}_c^{(g)}(t)$, for which $\mathbf{q}_c^{(g)}(t) \equiv \mathbf{0}$. The remaining DOFs pertain to $\mathbf{q}_u^{(g)}(t)$. Then, to ensure constraints are enforced, we can write the global equations of motion in partitioned form:

$$\begin{bmatrix} \mathbf{M}_{uu}^{(g)} & \mathbf{M}_{uc}^{(g)} \\ \mathbf{M}_{cu}^{(g)} & \mathbf{M}_{cc}^{(g)} \end{bmatrix} \begin{Bmatrix} \ddot{\mathbf{q}}_u^{(g)}(t) \\ \ddot{\mathbf{q}}_c^{(g)}(t) \end{Bmatrix} + \begin{bmatrix} \mathbf{K}_{uu}^{(g)} & \mathbf{K}_{uc}^{(g)} \\ \mathbf{K}_{cu}^{(g)} & \mathbf{K}_{cc}^{(g)} \end{bmatrix} \begin{Bmatrix} \mathbf{q}_u^{(g)}(t) \\ \mathbf{q}_c^{(g)}(t) \end{Bmatrix} = \begin{Bmatrix} \mathbf{Q}_u^{(g)}(t) \\ \mathbf{Q}_c^{(g)}(t) \end{Bmatrix}. \tag{64}$$

From the first block of equations, we see that:

$$\mathbf{M}_{uu}^{(g)}\ddot{\mathbf{q}}_u^{(g)}(t) + \mathbf{K}_{uu}^{(g)}\mathbf{q}_u^{(g)}(t) = \mathbf{Q}_u^{(g)}(t) - \mathbf{M}_{uc}^{(g)}\ddot{\mathbf{q}}_c^{(g)}(t) - \mathbf{K}_{uc}^{(g)}\mathbf{q}_c^{(g)}(t), \tag{65}$$

which is a set of linear, second-order, ordinary differential equations for $\mathbf{q}_u^{(g)}(t)$. If $\mathbf{q}_c^{(g)}(t)$ is prescribed, then $\ddot{\mathbf{q}}_c^{(g)}(t)$ is also known. The loads applied on the unconstrained DOFs, collected in $\mathbf{Q}_u^{(g)}(t)$, are also provided as an input, if one is dealing with a direct dynamic problem (i.e. if one wants to find the motion which results due to applied loads).

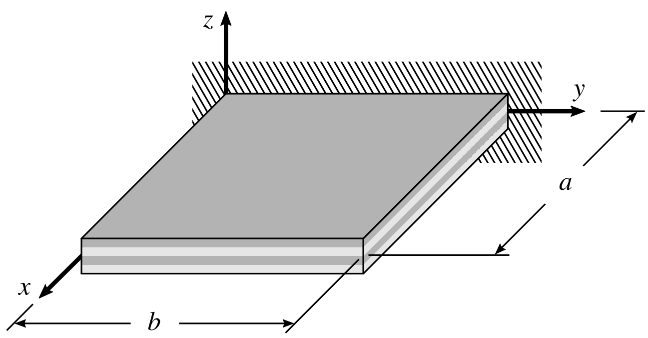

Figure 18: Laminate with four layers, clamped on one of its edges, considered in this section.

Once $\mathbf{q}_u^{(g)}(t)$ is known, then the second block of equations in (64) can be used to assess the reaction loads, which are required to constrain the DOFs in $\mathbf{q}_c^{(g)}(t)$ accordingly:

$$\mathbf{Q}_c^{(g)}(t) = \mathbf{M}_{cu}^{(g)}\ddot{\mathbf{q}}_u^{(g)}(t) + \mathbf{M}_{cc}^{(g)}\ddot{\mathbf{q}}_c^{(g)}(t) + \mathbf{K}_{cu}^{(g)}\mathbf{q}_u^{(g)}(t) + \mathbf{K}_{cc}^{(g)}\mathbf{q}_c^{(g)}(t). \tag{66}$$

For the clamp boundary condition, the previous equations simplify considerably, to provide:

$$\mathbf{M}_{uu}^{(g)}\ddot{\mathbf{q}}_u^{(g)}(t) + \mathbf{K}_{uu}^{(g)}\mathbf{q}_u^{(g)}(t) = \mathbf{Q}_u^{(g)}(t); \tag{67}$$

$$\mathbf{Q}_c^{(g)}(t) = \mathbf{M}_{cu}^{(g)}\ddot{\mathbf{q}}_u^{(g)}(t) + \mathbf{K}_{cu}^{(g)}\mathbf{q}_u^{(g)}(t). \tag{68}$$

Modal analysis The first type of dynamic analysis one might be interested in relates to the determination of natural frequencies and corresponding vibration mode shapes. These dynamic properties of a structural system fully characterize its behavior in the absence of externally applied loads. For obtaining them, one admits $\mathbf{Q}_u^{(g)}(t) = \mathbf{0}$, and that $\mathbf{q}_u^{(g)}(t) = \hat{\mathbf{q}}_u^{(g)}\mathrm{e}^{st}$, with s an undetermined scalar, and $\hat{\mathbf{q}}^{(g)}$ a vector of amplitudes. Substituting this ansatz on the equations of motion, we obtain:

$$\left[s^2\mathbf{M}_{uu}^{(g)} + \mathbf{K}_{uu}^{(g)}\right]\hat{\mathbf{q}}_u^{(g)} = \mathbf{0}, \tag{69}$$

which admits a non-trivial solution (i.e. for which $\hat{\mathbf{q}}_u^{(g)} \neq \mathbf{0}$) only if $\det\left[s^2\mathbf{M}_{uu}^{(g)} + \mathbf{K}_{uu}^{(g)}\right] = 0$. The previous equation, in fact, corresponds to an eigenvalue problem, with eigenvalues $s = j\omega$ and eigenvectors $\hat{\mathbf{q}}_u^{(g)}$, with $j = \sqrt{-1}$ the imaginary unit. The natural frequencies are given by ω, whereas vibration mode shapes are proportional to $\hat{\mathbf{q}}_u^{(g)}$. Depending on future analyzes which might be performed, and that rely on the so-called modal superposition technique, eigenmodes can be normalized, if desired.

Harmonic analysis In this case, one is interested in the steady-state response of the structure when it is subjected to harmonically-varying loads. We then consider $\mathbf{Q}_u^{(g)}(t) = \tilde{\mathbf{Q}}_u^{(g)}\mathrm{e}^{j\Omega t}$, with $\tilde{\mathbf{Q}}_u^{(g)}$ representing amplitudes and Ω the forcing frequency. If the system is linear, as considered here, then steady-state responses must occur with the same frequency as the one of the excitation, such that $\mathbf{q}_u^{(g)}(t) = \tilde{\mathbf{q}}_u^{(g)}\mathrm{e}^{j\Omega t}$, with $\tilde{\mathbf{q}}_u^{(g)}$ potentially being complex, to account for phase differences between responses and excitation (if damping is considered, for example). One then obtains:

$$\left(-\Omega^2\mathbf{M}_{uu}^{(g)} + \mathbf{K}_{uu}^{(g)}\right)\tilde{\mathbf{q}}_u^{(g)} = \tilde{\mathbf{Q}}_u^{(g)} \qquad \Rightarrow \qquad \tilde{\mathbf{q}}_u^{(g)} = \left(-\Omega^2\mathbf{M}_{uu}^{(g)} + \mathbf{K}_{uu}^{(g)}\right)^{-1}\tilde{\mathbf{Q}}_u^{(g)}. \tag{70}$$

Transient analysis When arbitrary external loads are applied to the structure, or initial conditions are given and the resulting motion is sought, then the ordinary differential equations of motion need to be integrated in time. This corresponds to a transient analysis, which can usually be performed by resorting to numerical integration algorithms, such as the Newmark method, the Runge-Kutta methods, the Hilber-Hughes-Taylor (HHT) method, etc. If the integration method is of first order, then the equations of motion (65) can be recast in the form:

$$\mathbf{A}\dot{\mathbf{z}}(t) + \mathbf{B}\mathbf{z}(t) = \mathbf{u}(t), \tag{71}$$

with:

$$\mathbf{A} = \begin{bmatrix} \mathbf{C}_{uu}^{(g)} & \mathbf{M}_{uu}^{(g)} \\ \mathbf{M}_{uu}^{(g)} & \mathbf{0} \end{bmatrix}; \qquad \mathbf{B} = \begin{bmatrix} \mathbf{K}_{uu}^{(g)} & \mathbf{0} \\ \mathbf{0} & -\mathbf{M}_{uu}^{(g)} \end{bmatrix}; \qquad \mathbf{z}(t) = \begin{Bmatrix} \mathbf{q}_u^{(g)}(t) \\ \dot{\mathbf{q}}_u^{(g)}(t) \end{Bmatrix};$$

$$\mathbf{u}(t) = \begin{Bmatrix} \mathbf{Q}_u^{(g)}(t) - \mathbf{M}_{uc}^{(g)}\ddot{\mathbf{q}}_c^{(g)}(t) - \mathbf{C}_{uc}^{(g)}\dot{\mathbf{q}}_c^{(g)}(t) - \mathbf{K}_{uc}^{(g)}\mathbf{q}_c^{(g)}(t) \\ \mathbf{0} \end{Bmatrix}, \tag{72}$$

which take into account contributions related to viscous damping, through partitions of the global damping matrix $\mathbf{C}^{(g)}$, seen in the expressions put forward for $\mathbf{A}$ and $\mathbf{u}$.

Besides, as discussed in the introduction of this chapter, various strategies can be considered to reduce computation time and/or alleviate memory allocation demanded by a transient analysis. One of such strategies, which is known as modal superposition, consists in representing the unknown solution as a weighted sum of the structure mode shapes. Typically, the number of wave modes adopted in this setting is much smaller than the original, complete number of global DOFs of the finite element mesh. Because the number of unknowns gets reduced, the equations of motion are also projected onto the vector space spanned by the wave modes used to represent the response, aiming to reduce the error of the approximation. If the wave modes used to represent the responses are grouped in a matrix $\mathbf{T}$, then one can write $\boldsymbol{\eta}(t) = \mathbf{T}\mathbf{q}_u^{(g)}(t)$, with the size of $\boldsymbol{\eta}(t)$ much smaller than the size of $\mathbf{q}_u^{(g)}(t)$. Variables grouped in $\boldsymbol{\eta}$ are commonly named *modal coordinates*. In the modal superposition setting, Eq. (71) remains valid, as long as quantities given in Eq. (72) are redefined according to:

$$\mathbf{A} = \begin{bmatrix} \mathbf{T}^{\mathrm{T}}\mathbf{C}_{uu}^{(g)}\mathbf{T} & \mathbf{T}^{\mathrm{T}}\mathbf{M}_{uu}^{(g)}\mathbf{T} \\ \mathbf{T}^{\mathrm{T}}\mathbf{M}_{uu}^{(g)}\mathbf{T} & \mathbf{0} \end{bmatrix}; \qquad \mathbf{B} = \begin{bmatrix} \mathbf{T}^{\mathrm{T}}\mathbf{K}_{uu}^{(g)}\mathbf{T} & \mathbf{0} \\ \mathbf{0} & -\mathbf{T}^{\mathrm{T}}\mathbf{M}_{uu}^{(g)}\mathbf{T} \end{bmatrix}; \qquad \mathbf{z}(t) = \begin{Bmatrix} \boldsymbol{\eta}(t) \\ \dot{\boldsymbol{\eta}}(t) \end{Bmatrix};$$
$$\mathbf{u}(t) = \begin{Bmatrix} \mathbf{T}^{\mathrm{T}}\left[\mathbf{Q}_u^{(g)}(t) - \mathbf{M}_{uc}^{(g)}\ddot{\mathbf{q}}_c^{(g)}(t) - \mathbf{C}_{uc}^{(g)}\dot{\mathbf{q}}_c^{(g)}(t) - \mathbf{K}_{uc}^{(g)}\mathbf{q}_c^{(g)}(t)\right] \\ \mathbf{0} \end{Bmatrix}. \quad (73)$$

At this point, one note that the laminate considered in this example has been discretized using a mesh with 15×15 elements. This mesh therefore comprises 256 nodes and 1280 DOFs (with five DOFs per node, cf. the finite element formulation discussed in section 2.2), prior to enforcing the clamp constraint. The number of unconstrained DOFs equals 1200.

By performing a modal analysis, one obtained the first 10 natural frequencies of the considered laminate, which are reported in Tab. 6. The corresponding vibration mode shapes can be visualized in Fig. 19. Notice that, for all modes, the edge of the laminate at $x = 0$ does not move, in accordance with the specified boundary condition.

Table 6: Natural frequencies of the laminate considered in this section.

n	1	2	3	4	5	6	7	8	9	10
$\frac{1}{2\pi}\omega_n$ [Hz]	6.85	24.9	39.7	65.6	81.6	123.8	137.3	154.3	170.1	241.0

A harmonic analysis is also carried out. The external load is a force acting along z, with unit magnitude, $\vec{F} = 1\vec{k}$ [N], on the node located at $x = a$, $y = b$. It is duly incorporated into the adequate row of $\tilde{\mathbf{Q}}_u^{(g)}$. The response is obtained at the same node, corresponding to its transverse displacement DOF. The forcing frequency is varied from 0 to 200 Hz, in 800 increments. The harmonic response is shown in Fig. 20, in the form of a Bode plot.

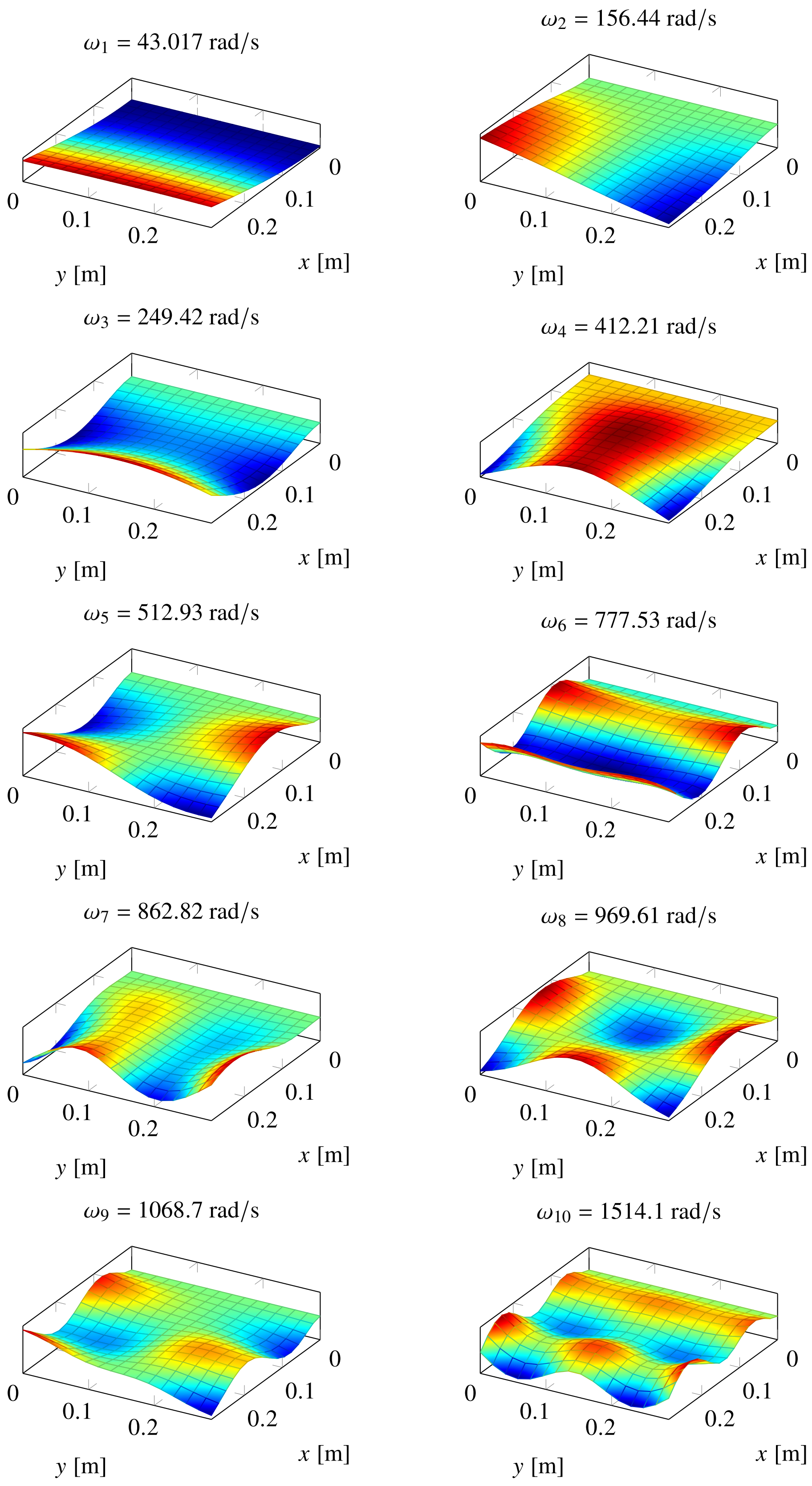

Figure 19: Vibration mode shapes (eigenvectors) of the laminate considered in this section.

Finally, a result related to a transient analysis is also reported. For this investigation, it has been assumed that a force $\vec{F} = \bar{F}(t)\vec{k}$ was applied at the node located at $x = a$, $y = 0$, with the magnitude $\bar{F}(t)$ corresponding to a triangular pulse with amplitude 1 N and duration of 20 ms, as shown in Fig. 21. The initial conditions were assumed to be null. Also, the mode superposition approach was considered for integrating the equations of motion. The first 30 mode shapes were used to approximate the unknowns. The largest natural frequency of the former is roughly equal to 746.4 Hz. It is usually recommended for one to include all modes bellow at least twice the maximum frequency of interest in the transformation matrix $\mathbf{T}$ used in the modal superposition approach [Craig and Kurdila, 2006]. Based on this premise, obtained responses should be relatively accurate for as long as the frequency content of the excitation load remains below, say, 373 Hz. The spectrum of $\bar{F}(t)$ illustrated in Fig. 21 indicates that this is not entirely true – so obtained results may not be completely correct.

For computing the transient response, a discrete viscous damper was also included in the model. It was placed between the node at $x = 8a/15 \cong 153.07$ mm, $y = 8b/15 \cong 153.07$ mm (close to the center of the laminate) and the ground. Also, the damper was assumed to dissipate energy based on the transverse motion of the corresponding node of the mesh, based on a viscous damping coefficient equal to $0.5\,\mathrm{N\,s\,m^{-1}}$. The damping matrix $\mathbf{C}^{(g)}$ therefore is almost entirely zero, except for the diagonal entry related to the transverse displacement w DOF of the node to which the damper is attached.

A single response of the laminate due to the transient excitation load is depicted here, in Fig. 22. It corresponds to the transverse displacement of the node located at $x = a$, $y = b$. As one can see, some vibration induced by the external load gets mitigated by the damper. The laminate continues

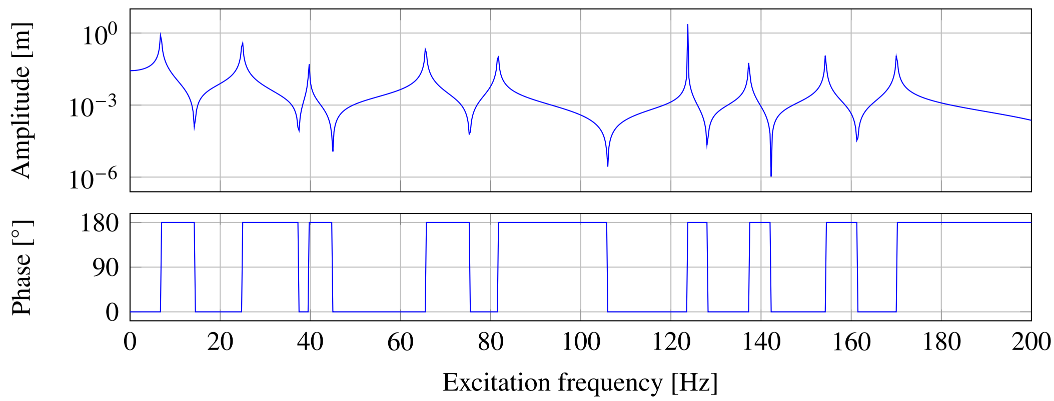

Figure 20: Harmonic response (transverse displacement DOF) at the driving point $x = a$, $y = b$ of the laminate considered in this section.

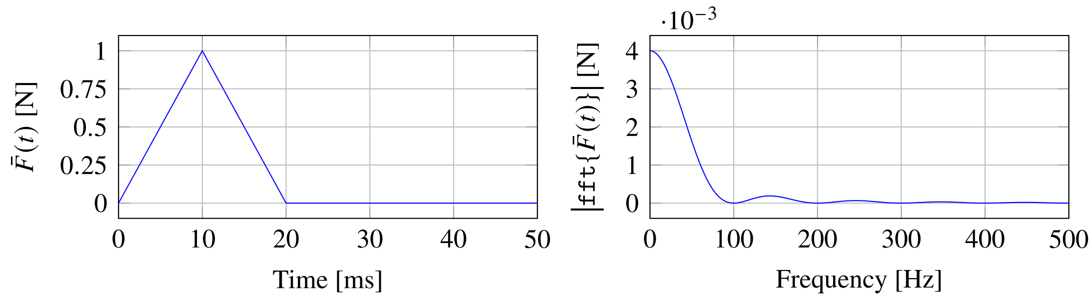

Figure 21: Time history (left) and spectrum (right) of the force amplitude $\bar{F}$ adopted for the transient analysis of the laminate considered in this section.

to vibrate somewhat, however, due to the damper not being able to adequately attenuate motion related to particular wave modes of the structure. A low decay rate can still be seen, even for such condition. We remark that the time integration algorithm used to obtain the result shown in Fig. 22 should not be responsible for the observed damping.

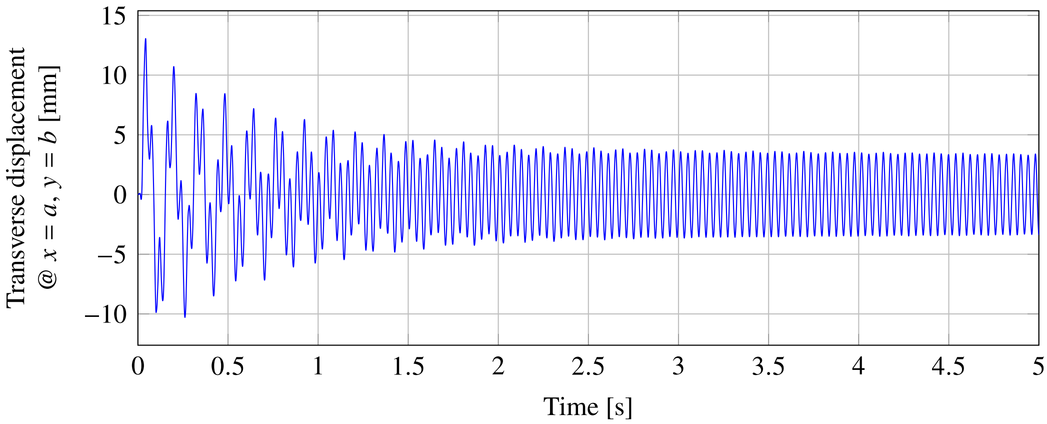

Figure 22: Transverse displacement of the point at $x = a$, $y = b$ of the laminate considered in this section, when it is subjected to the transverse force given in Fig. 21 at $x = a$, $y = 0$.

4 Parameterization of FE models for model updating and damage identification

Most often, the finite element modeling of complex engineering systems involves uncertainties affecting some physical or geometrical parameters (material parameters, geometrical dimensions, etc.). Other sources of uncertainties are boundary conditions and internal joints, the properties of which, due to the presence of contact, are difficult to characterize.

Hence, to reduce the errors involved in FE modeling, and obtain models sufficiently accurate to ensure reliable predictions, one strategy consists in performing the so-called *model updating* of an initial FE model. This can be achieved by performing experimental tests on the real structure (when it is available) and then introducing corrections in the FE model in such a way to minimize, as much as possible, the differences between a set of experimental responses and the corresponding model predictions. For this goal, since it is not reasonable to adjust the properties of each element of the mesh individually, it is convenient to assume the structure divided in a certain number of regions (macro-elements), and assign correction factors to the stiffness and/or inertia of each of these regions. Such an approach enables to consider modeling errors in terms of a reduced number of parameters, associated to the regions assumed to concentrate the dominant modeling errors. The model updating problem can thus be formulated as an optimization problem in which the objective function represents the difference between experimental responses and model predictions, and the design variables are the correction factors to be applied to the macro-elements of the model.

Considering problems in the field of structural dynamics, we recall the global equations of motion in the form:

$$\mathbf{M}^{(g)}\ddot{\mathbf{q}}^{(g)}(t) + \mathbf{K}^{(g)}\mathbf{q}^{(g)}(t) = \mathbf{Q}_{\mathrm{nc}}^{(g)}(t) + \mathbf{Q}_{b}^{(g)}(t) + \mathbf{Q}_{s}^{(g)}(t). \tag{74}$$

Assuming the structure divided in p regions, the mass and stiffness correction matrices to be introduced in the updated FE model can be represented as follows:

$$\Delta\mathbf{M}^{(g)} = \bigcup_{r=1}^{R_m} m_r \mathbf{M}^{(r)}, \tag{75a}$$

$$\Delta\mathbf{K}^{(g)} = \bigcup_{r=1}^{R_k} k_r \mathbf{K}^{(r)}, \tag{75b}$$

where $\mathbf{M}^{(r)}$ and $\mathbf{K}^{(r)}$ are, respectively, the mass and stiffness contributions of region r to the corresponding global matrices, m_r and k_r are the associated correction parameters, and symbol $\bigcup$ indicates the operation of matrix assembling. Also, R_m and R_k stand for the number of different regions which are considered for correcting the mass and stiffness matrices, respectively.

A similar approach can be used for model-based damage identification, in which damage is assumed to be represented by error indicators, assigned to the probable damaged regions of the structure. The damage identification problem then consists in determining the set of damage indicators which makes the FE model to reproduce the experimentally measured responses of the damaged structure.

Different strategies for FE model updating and damage identification based on structural dynamic responses have been developed [Friswell and Mottershead, 1995]. In the next section, a classical approach, based on the sensitivity of eigenvalues and eigenvectors, is described.

5 Model updating based on the sensitivity of eigenvalues and eigenvectors

Neglecting damping, and assuming that S pairs of experimental eigensolutions – natural frequencies and natural vibration modes, ($\omega_s^{(\mathrm{exp})} \in \mathbb{R}$, $\mathbf{X}_s^{(\mathrm{exp})} \in \mathbb{R}^c$, $s = 1, \dots, S$) – are available, the approach starts by expressing the eigensolutions as linearized Taylor series expansions about the corresponding ones obtained from the FE model ($\lambda_s^{(m)} = {\omega_s^{(m)}}^2$, $\mathbf{X}_s^{(m)}$, $s = 1, \dots, S$):

$$\lambda_s^{(\mathrm{exp})} = \lambda_s^{(m)} + \sum_{r=1}^{R_m} \frac{\partial \lambda_r^{(m)}}{\partial m_r}\Delta m_r + \sum_{r=1}^{R_k} \frac{\partial \lambda_r^{(m)}}{\partial k_r}\Delta k_r, \qquad s = 1, 2, \dots, S, \tag{76a}$$

$$\mathbf{X}_s^{(\mathrm{exp})} = \mathbf{X}_s^{(m)} + \sum_{r=1}^{R_m} \frac{\partial \mathbf{X}_r^{(m)}}{\partial m_r}\Delta m_r + \sum_{r=1}^{R_k} \frac{\partial \mathbf{X}_r^{(m)}}{\partial k_r}\Delta k_r, \qquad s = 1, 2, \dots, S. \tag{76b}$$

It should be explained that, in the equations above, $\mathbf{X}_s^{(\mathrm{exp})} \in \mathbb{R}^c$, for $s = 1, 2, \dots, S$, are sub-eigenvectors formed only by the c components identified during experimental tests (e.g. from experimental modal analysis), while $\mathbf{X}_s^{(m)} \in \mathbb{R}^c$, for $s = 1, 2, \dots, S$ are the counterparts provided by the FE model.

Since the parameters m_r and k_r intervene nonlinearly in the eigensolutions, their determination has to be done iteratively by solving Eqs. (76) for the increments Δm_r and Δk_r, starting from initial guessed values. In each iteration, the following linear system of equations has to be solved:

$$\begin{Bmatrix} \Delta\lambda_1 \\ \vdots \\ \Delta\lambda_S \\ \Delta\mathbf{X}_1 \\ \vdots \\ \Delta\mathbf{X}_S \end{Bmatrix} = \begin{bmatrix} \frac{\partial \lambda_1^{(m)}}{\partial m_1} & \cdots & \frac{\partial \lambda_1^{(m)}}{\partial m_{R_m}} & \frac{\partial \lambda_1^{(m)}}{\partial k_1} & \cdots & \frac{\partial \lambda_1^{(m)}}{\partial k_{R_k}} \\ \vdots & \ddots & \vdots & \vdots & \ddots & \vdots \\ \frac{\partial \lambda_S^{(m)}}{\partial m_1} & \cdots & \frac{\partial \lambda_S^{(m)}}{\partial m_{R_m}} & \frac{\partial \lambda_S^{(m)}}{\partial k_1} & \cdots & \frac{\partial \lambda_S^{(m)}}{\partial k_{R_k}} \\ \frac{\partial \mathbf{X}_1^{(m)}}{\partial m_1} & \cdots & \frac{\partial \mathbf{X}_1^{(m)}}{\partial m_{R_m}} & \frac{\partial \mathbf{X}_1^{(m)}}{\partial k_1} & \cdots & \frac{\partial \mathbf{X}_1^{(m)}}{\partial k_{R_k}} \\ \vdots & \ddots & \vdots & \ddots & \vdots & \vdots \\ \frac{\partial \mathbf{X}_S^{(m)}}{\partial m_1} & \cdots & \frac{\partial \mathbf{X}_S^{(m)}}{\partial m_R} & \frac{\partial \mathbf{X}_S^{(m)}}{\partial k_1} & \cdots & \frac{\partial \mathbf{X}_S^{(m)}}{\partial k_{R_k}} \end{bmatrix} \begin{Bmatrix} \Delta m_1 \\ \vdots \\ \Delta m_{R_m} \\ \Delta k_1 \\ \vdots \\ \Delta k_{R_k} \end{Bmatrix} \tag{77}$$

or

$$\Delta\mathbf{L} = \mathbf{S}\,\Delta\mathbf{P}. \tag{78}$$

As long as the number of equations $(S(1+c))$ is larger than the number of unknowns $(R_m + R_k)$ and matrix $\mathbf{S}$ is full-rank, the system of equations has a unique least-square solution:

$$\Delta\mathbf{P} = \left(\mathbf{S}^{\mathrm{T}}\mathbf{S}\right)^{-1}\mathbf{S}^{\mathrm{T}}\Delta\mathbf{L}. \tag{79}$$

Matrix $\mathbf{S}$ is formed by the sensitivities of the eigensolutions with respect to the correction parameters. As stated in [Friswell and Mottershead, 1995], different methods have been devised to compute those sensitivities.

Given the undamped eigenvalue problem associated to Eq. (74),

$$\left[\mathbf{K}^{(g)} - \lambda_s\mathbf{M}^{(g)}\right]\mathbf{X}_s = \mathbf{0}, \tag{80}$$

the derivation with respect to a given mass m_r or stiffness correction parameter k_r leads, respectively, to

$$\left[\mathbf{K}^{(g)} - \lambda_s\mathbf{M}^{(g)}\right]\frac{\partial\mathbf{X}_s}{\partial m_r} = -\left[\lambda_s\frac{\partial\mathbf{M}^{(g)}}{\partial m_r} + \frac{\partial\lambda_s}{\partial m_r}\mathbf{M}^{(g)}\right]\mathbf{X}_s, \qquad s = 1, 2, \ldots, S, \tag{81a}$$

$$\left[\mathbf{K}^{(g)} - \lambda_s\mathbf{M}^{(g)}\right]\frac{\partial\mathbf{X}_s}{\partial k_r} = \left[\frac{\partial\mathbf{K}^{(g)}}{\partial k_r} - \frac{\partial\lambda_s}{\partial k_r}\mathbf{M}^{(g)}\right]\mathbf{X}_s, \qquad s = 1, 2, \ldots, S. \tag{81b}$$

Assuming that the derivative of the s-th eigenvector can be projected on the basis formed by a set of Q eigenvectors, one writes:

$$\frac{\partial\mathbf{X}_s}{\partial m_r} = \sum_{q=1}^{Q}\mathbf{X}_q c_{sq}^r, \tag{82a}$$

$$\frac{\partial\mathbf{X}_s}{\partial k_r} = \sum_{q=1}^{Q}\mathbf{X}_q d_{sq}^r. \tag{82b}$$

Associating Eqs. (81) and (82), pre-multiplying both sides of the resulting equations by the eigenvector $\mathbf{X}_s$, which is assumed to be normalized to unit modal mass, one obtains the following expressions for the sensitivity of the r-th eigenvalue with respect to the mass and stiffness correction parameters, respectively:

$$\frac{\partial\lambda_s}{\partial m_r} = -\lambda_s\mathbf{X}_s^{\mathrm{T}}\frac{\partial\mathbf{M}^{(g)}}{\partial m_r}\mathbf{X}_s = -\lambda_s\mathbf{X}_s^{\mathrm{T}}\mathbf{M}^{(r)}\mathbf{X}_s, \tag{83a}$$

$$\frac{\partial\lambda_s}{\partial k_r} = \mathbf{X}_s^{\mathrm{T}}\frac{\partial\mathbf{K}^{(g)}}{\partial k_r}\mathbf{X}_s = \mathbf{X}_s^{\mathrm{T}}\mathbf{K}^{(r)}\mathbf{X}_s. \tag{83b}$$

Regarding Eqs. (83), it is worth pointing-out that the computation of the sensitivity of the s-th eigenvalue is straightforward and depends on the s-th eigenvector, only.

The computation of the sensitivities of the eigenvectors is somewhat more involved. The fundamental idea is to determine the expressions for the coefficients c_{sq}^r and d_{sq}^r in Eqs. (82). This is done by first deriving the normalization equations for the eigenvectors with respect to the correction parameters, as indicated next:

$$\mathbf{X}_s^{\mathrm{T}}\mathbf{M}^{(g)}\mathbf{X}_s = 1 \qquad \Rightarrow \qquad \mathbf{X}_s^{\mathrm{T}}\frac{\partial\mathbf{M}^{(g)}}{\partial m_r}\mathbf{X}_s + 2\mathbf{X}_s^{\mathrm{T}}\mathbf{M}^{(g)}\frac{\partial\mathbf{X}_s}{\partial m_r} = 0, \tag{84a}$$

$$\mathbf{X}_s^{\mathrm{T}}\mathbf{K}^{(g)}\mathbf{X}_s = \lambda_s \qquad \Rightarrow \qquad \mathbf{X}_s^{\mathrm{T}}\frac{\partial\mathbf{K}^{(g)}}{\partial k_r}\mathbf{X}_s + 2\mathbf{X}_s^{\mathrm{T}}\mathbf{K}^{(g)}\frac{\partial\mathbf{X}_s}{\partial k_r} = \frac{\partial\lambda_s}{\partial k_r}. \tag{84b}$$

Making use of Eqs. (82) and (83) and the orthogonality relations of the eigenvectors, one gets:

$$c_{ss}^r = -\frac{1}{2}\mathbf{X}_s^T\mathbf{M}^{(r)}\mathbf{X}_s, \tag{85a}$$

$$d_{ss}^r = 0. \tag{85b}$$

The determination of the remaining coefficients c_{qs}^r and d_{qs}^r with $r \neq s$ requires the use of Eqs. (81) in combination with Eqs. (82) and, again, the orthogonality relations of the eigenvectors. This procedure leads to the following expressions:

$$c_{sq}^r = \lambda_s \frac{\mathbf{X}_q^{\mathrm{T}}\mathbf{M}^{(r)}\mathbf{X}_s}{\lambda_q - \lambda_s}, \qquad r \neq s, \tag{86a}$$

$$d_{sq}^r = -\frac{\mathbf{X}_q^{\mathrm{T}}\mathbf{K}^{(r)}\mathbf{X}_s}{\lambda_q - \lambda_s}, \qquad r \neq s. \tag{86b}$$

Regarding the method presented above, it is worth highlighting its following features:

a) it requires one-to-one pairing between the natural frequencies and natural vibration modes obtained experimentally with those computed from the FE model. This can be a difficult task, especially when the modeling errors are large enough so as to render direct comparison ineffective for pairing. Hence, a number of numerical techniques have been devised to assist the comparison between the two sets of eigensolutions, such as the Modal Assurance Criterion (MAC) and the Coordinate Modal Assurance Criterion (COMAC) [e Silva and Maia, 2012];

b) as the components of the experimental and FE eigenvectors are directly paired, the method does not require the condensation of the FE model to ensure dimensional compatibility of both sets of eigenvectors.

c) it follows a fully deterministic approach, which means that random noise affecting the measured quantities or modeling errors are not considered. However, it is possible to formulate the model updating in a stochastic framework, where various estimators, can be used to deal with random uncertainties [Fonseca et al., 2005, Mares et al., 2006, Simoen et al., 2013].

6 Final remarks

The finite element method is, undoubtedly, a very powerful method, which has been playing a significant role in scientific and technological developments lately. However, in the authors' opinion, users must be fully aware, not only of its capabilities, but also of its limitations. In fact, it is widely recognized that modeling of complex systems is a combination of science and art, meaning that it is never a fully automated procedure, requiring, from the user: a) knowledge of the physics underlying the problem at hand, necessary to make adequate modeling choices and correct interpretation of the results; b) knowledge of the various resources available in commercial packages (in case these are used), necessary for the construction of representative, accurate and cost-effective models for the problem at hand; c) expert judgement, obtained from previous experience gathered in the modeling of similar problems.

It should be mentioned that, in many cases of scientific or industrial interest, FE models are constructed for use in combination with other numerical analyses, in broader frameworks. As relevant examples, one can cite:

- **Structural optimization:** a finite element model of a given structure is coupled to numerical optimization routines aiming at improving one or a set of desired responses or structural characteristics. In this case, the degree to which the improvement is obtained is quantified by one or various *cost functions* or *objective functions*, and the structural features to be modified form a set of *design variables*. Most often, the optimization problem is subject to the so-called *constraints*, which limit the range of possible solutions (design space). Generally, optimization problems must be solved iteratively, the FE model being used to compute the value of the objective and other necessary quantities at each iteration;

- **Uncertainty quantification:** a single FE model of a given structure is inherently, a deterministic model. As the modeling of complex systems most frequently involve uncertainties affecting external loads and physical and geometrical characteristics of the structure, it is of utmost importance, in many situations, to assess how those uncertainties can influence the responses predicted by the FE model. In a probabilistic scope, the immediate assessment can be made by the Monte Carlo method, which consists in generating a typically large number of samples of the assumed random variables and, for each sample, compute a corresponding response sample. These later can then be used to compute statistics of the structural responses, which, to have ensured statistical confidence, require a large number of samples and, as a result, of FE response evaluations. Other relevant problems related to uncertainty quantification are the assessment of structural reliability [Ditlevsen and Madsen, 1996] and robust optimization [Ben-Tal et al., 2009].

- **Damage identification:** this problem can be included in the more general scope of model-based parameter identification problems. More specifically, it can be regarded as a dual problem of model updating, described in section 5, as long as the correction coefficients are interpreted as damage indicators [Friswell, 2007, Fan and Qiao, 2011].

- **Sensitivity analysis:** this type of numerical analysis aims at assessing the degrees to which the structural responses of interest are influenced by variations of certain physical and/or geometrical structural characteristics [Saltelli et al., 2008]. This analysis is highly useful in structural design and also in other applications, such as structural optimization and uncertainty propagation.

References

K.-J. Bathe. *Finite Element Procedures*. Klaus-Jürgen Bathe, Watertown, MA, Jan. 2014. ISBN 978-0-9790049-5-7.

A. Ben-Tal, L. El Ghaoui, and A. Nemirovski. *Robust optimization*, volume 28. Princeton university press, 2009.

P. Chen and C. Schwab. Model order reduction methods in computational uncertainty quantification. In *Handbook of Uncertainty Quantification*, pages 937–990. Springer International Publishing, 2017. doi: 10.1007/978-3-319-12385-1_70. URL https://doi.org/10.1007/978-3-319-12385-1_70.

J. A. Cottrell, T. J. R. Hughes, and Y. Bazilevs. *Isogeometric analysis*. Wiley-Blackwell, Hoboken, NJ, Aug. 2009.

R. R. Craig and A. J. Kurdila. *Fundamentals of structural dynamics*. John Wiley & Sons, Nashville, TN, 2 edition, June 2006.

R. de Borst, M. A. Crisfield, J. J. C. Remmers, and C. V. Verhoosel. *Nonlinear finite element analysis of solids and structures*. Wiley Series in Computational Mechanics. Wiley-Blackwell, Hoboken, NJ, 2 edition, Aug. 2012.

O. Ditlevsen and H. O. Madsen. *Structural reliability methods*, volume 178. Wiley New York, 1996.

J. M. M. e Silva and N. M. Maia. *Modal analysis and testing*, volume 363. Springer Science & Business Media, 2012.

W. Fan and P. Qiao. Vibration-based damage identification methods: a review and comparative study. *Structural health monitoring*, 10(1):83–111, 2011.

J. R. Fonseca, M. I. Friswell, J. E. Mottershead, and A. W. Lees. Uncertainty identification by the maximum likelihood method. *Journal of Sound and Vibration*, 288(3):587–599, 2005.

M. Friswell and J. E. Mottershead. *Finite element model updating in structural dynamics*, volume 38. Springer Science & Business Media, 1995.

M. I. Friswell. Damage identification using inverse methods. *Philosophical Transactions of the Royal Society A: Mathematical, Physical and Engineering Sciences*, 365(1851):393–410, 2007.

Y. C. Fung, P. Tong, and X. Chen. *Classical and Computational Solid Mechanics*. WORLD SCIENTIFIC, July 2017. doi: 10.1142/9744. URL https://doi.org/10.1142/9744.

L. L. Gratiet, S. Marelli, and B. Sudret. Metamodel-based sensitivity analysis: Polynomial chaos expansions and gaussian processes. In *Handbook of Uncertainty Quantification*, pages 1289–1325. Springer International Publishing, 2017. doi: 10.1007/978-3-319-12385-1_38. URL https://doi.org/10.1007/978-3-319-12385-1_38.

J.-M. Jin. *The finite element method in electromagnetics*. John Wiley & Sons, 2015.

C. D. M. Junior, A. Erturk, and D. J. Inman. An electromechanical finite element model for piezoelectric energy harvester plates. *Journal of Sound and Vibration*, 327(1-2):9–25, Oct. 2009. doi: 10.1016/j.jsv.2009.05.015. URL https://doi.org/10.1016/j.jsv.2009.05.015.

C. Lanczos. *The variational principles of mechanics*. Dover Books on Physics. Dover Publications, Mineola, NY, Mar. 1986.

R. W. Lewis, K. Morgan, H. Thomas, and K. N. Seetharamu. *The finite element method in heat transfer analysis*. John Wiley & Sons, 1996.

C. Mares, J. Mottershead, and M. Friswell. Stochastic model updating: part 1—theory and simulated example. *Mechanical systems and signal processing*, 20(7):1674–1695, 2006.

D. Pereira, T. Guimarães, H. Resende, and D. Rade. Numerical and experimental analyses of modal frequency and damping in tow-steered CFRP laminates. *Composite Structures*, 244: 112190, July 2020. doi: 10.1016/j.compstruct.2020.112190. URL https://doi.org/10.1016/j.compstruct.2020.112190.

J. N. Reddy. *Mechanics of laminated composite plates and shells*. CRC Press, Boca Raton, FL, 2 edition, Nov. 2003.

J. N. Reddy. *Introduction to the finite element method*. McGraw-Hill Education, 2019.

A. Saltelli, M. Ratto, T. Andres, F. Campolongo, J. Cariboni, D. Gatelli, M. Saisana, and S. Tarantola. Introduction to sensitivity analysis. *Global sensitivity analysis. The primer*, pages 1–51, 2008.

K. Sargsyan. Surrogate models for uncertainty propagation and sensitivity analysis. In *Handbook of Uncertainty Quantification*, pages 673–698. Springer International Publishing, 2017. doi: 10.1007/978-3-319-12385-1_22. URL https://doi.org/10.1007/978-3-319-12385-1_22.

E. Simoen, C. Papadimitriou, and G. Lombaert. On prediction error correlation in bayesian model updating. *Journal of Sound and Vibration*, 332(18):4136–4152, 2013.

R. Weinstock. *Calculus of Variations*. Dover Books on Mathematics. Dover Publications, Mineola, NY, July 1975.

O. C. Zienkiewicz, R. L. Taylor, and J. Z. Zhu. *The finite element method: Its basis and fundamentals*. The Finite Element Method. Butterworth-Heinemann, Oxford, England, 7 edition, Oct. 2013.

W. B. Zimmerman. *Multiphysics modeling with finite element methods*, volume 18. World Scientific Publishing Company, 2006.

Q. Zu-Qing. *Model order reduction techniques with applications in finite element analysis*. Springer, London, England, 2004 edition, Aug. 2004.